RESPONSES to comments of Anonymous Referee #1

This work is an attempt to constrain the BC emissions at high northern latitudes starting from four different inventories and applying a Bayesian inversion to the model Flexpart. The choices of emission inventories, of the surface stations and of ancilliary BC data to independently optimize BC emissions are well explained. Additional information is gained through varying below-cloud and in-cloud scavenging to adapt BC-like tracers that are used to improve the a-posteriori BC concentrations simulated by Flexpart. This paper is well structured, the approach is interesting and the results are pertinent. I suggest that is can be published after several improvements to the wording that are outlined below. I also have a few suggestions for reinforcing the discussion.

RESPONSE: We would like to acknowledge reviewer for his positive comments on our paper and his kind willingness to help improving this manuscript. We have tried to follow all of his suggestions.

Lines 314-315 page 11: "The different scavenging coefficients used did not create a large variation in the monthly concentrations of BC. The best performance for the majority of the stations examined and most months was obtained for species 1, 2 and 10 (see Table 2)." This is a rather surprising result since wet scavenging is the main global sink for BC. Does that indicate that dry deposition is an important process for removing BC at high northern latitude, in that case why didn't the authors vary the efficiency of dry scavenging as well as we scavenging? This aspect deserves several sentences in order to develop why the authors obtained such quantitative result.
RESPONSE: The reviewer has a good point in his comment. However, still dry deposition is only 20% of the total as in most global models.
The small variability stems from the small perturbation of the wet scavenging parameters. When changing scavenging parameters of BC, except for conducting a sensitivity analysis and estimate uncertainty, our top priority was to select the best representative species for BC, hence scavenging coefficients should be realistic. This resulted in the aforementioned small variability. Of course, if we change these parameters drastically, the variability will increase, but then we do not have realistic values anymore. We have now tried to clarify this in the text (please check manuscript with Track Changes).

Figure 7 show that vertical profiles can be optimized by the Bayesian approach. Schwartz et al. (2013) illustrate well that modelled BC concentrations profiles are systematically overestimated in the mid- to high- troposphere over the remote Pacific. The biases are much less pronounced over source regions. What can be learned from this work about improving the model performances over remote regions?
RESPONSE: The Bayesian approach forces emissions mathematically, in order to better match observations. Like we explain in section 3.4, the comparison to observations included in the inversion is not a sufficient indicator of the inversion's performance, as the inversion is designed to reduce the model-observation mismatches. The magnitude of the posterior reduction of the model mismatch to the observations is partly determined by the weighting given to the observations relative to the prior emissions. A much better performance indicator is the comparison of the posterior concentrations with observations that were not included in the inversion (independent observations).

For this reason, we have chosen to compare our posterior emissions with profiles from the ACCACIA campaign, which were not included in the inversion, and they were available in public for year 2013. We did exactly the same for years 2014 and 2015. So, the use of these profiles was for validation only.
Now, likewise in Schwartz et al. (2013) paper, our model overestimates up to 3 times concentrations of BC at lower altitudes, while this overestimation becomes more intense at higher altitudes. What we claim in the paper is that the observed model overestimation decreases drastically when using the resulting a posteriori emissions that were calculated from our Bayesian inversion framework (based on ground-based measurements).

In the abstract, I recommend that the authors substitute "posterior emissions" with "a-posteriori emission estimates" since at this stage the reader does not know what "posterior emissions" refers to.
RESPONSE: We very well agree and have corrected the manuscript (see manuscript with Track Changes).

Reference: Schwarz JP, Samset BH, Perring AE, et al. Global-scale seasonally re- solved black carbon vertical profiles over the Pacific.Âa˘Geophysical Research Letters. 2013;40(20):5542-5547. doi:10.1002/2013GL057775.

Minor comments:

Page 10, line 265: NSD was never defined before, I assume it refers to 'Normalized Standard Deviation" but the reader should not have to guess.

RESPONSE: We appreciate for this comment. We also noticed that nRMSE is not defined in the same paragraph. We have now corrected both (see manuscript with Track Changes).

Page 12, lines 334 & 337: the stations BOS (Bösel) and WLD (Whaldof) are discussed but not shown in Fig. S3
RESPONSE: As shown in Table 1, 17, 13 and 24 stations with continuous measurements were used for 2013, 2014 and 2015, respectively. It is not possible to show the results for all of them. Therefore we decided to show the northernmost stations. However, if we only comment on what we show, we are only telling half of the truth. Specifically, commenting on what it is shown only would result on missing a very important statement that all prior emission datasets failed to reproduce the observations in central Europe during all years studied (2013, 2014 and 2015) implying either missing sources or highly uncertain measurements (end of second paragraph of section 3.2).

Page 12, line 343: change "by 23% at maximum" to "by a maximum of 23%"
RESPONSE: Corrected (see manuscript with Track Changes).

Page 12, lines 344-353: change: "NMSE values calculated for each of the four emission inventories were very low at the majority of the stations for which data existed in all the years of study (ZEP, SUM, TIK, BAR, MEL and LEI), when ECLIPSEv5 emissions were used, while at PAL all emission datasets performed well (Figure 5). At most of the Arctic stations, the simulations using ECLIPSEv5 reproduced the observations better

compared to the other inventories examined. This shows that the most appropriate emission dataset for our purpose is the ECLIPSEv5 inventory, as it is the only one that can capture the characteristically elevated concentrations of BC in the Arctic, which persist until spring, and are caused by anthropogenic emissions (Law and Stohl, 2007). A significant deficiency is found for TIK for reasons that were explained earlier (see section 3.1)." to "Normalized mean square error values calculated for each of the four emission inventories were very low at the majority of the stations for which data existed in all the years of study (ZEP, SUM, TIK, BAR, MEL and LEI), when ECLIPSEv5 emissions were used. In contrast, at PAL all emission datasets performed well (Figure 5). The observations of BC concentrations at Arctic stations were better reproduced in simulations using the ECLIPSEv5 than with any other inventories examined. Law and Stohl (2007) have documented that these elevated BC concentrations are caused by anthropogenic emissions. Black carbon concentrations at TIK are not well simulated for reasons given in section 3.1."
RESPONSE: Corrected according to reviewer's suggestion (see manuscript with Track Changes).

Page 13, lines 366-367: change "Table 3 reports annual prior and posterior emissions of BC for different regions and 367 average emissions for the period 2013–2015." To "Table 3 reports annual prior, posterior, and averaged over 2013-2015, BC emissions for different regions."
RESPONSE: We have also corrected this sentence (please see manuscript with Track Changes).

Page 13, line 371 and everywhere in the remaining text: change "emissions of BC" to "BC emissions".
RESPONSE: We have corrected the expression from page 13 onwards. To keep a level of diversity in the manuscript, we have kept the expression as it was before ("emissions of BC") in the titles of sections and in the legends of figures (please see manuscript with Track Changes).

Page 14, line 410-411: change "The relative uncertainty of the inversion averaged over the period 2013 to 2015 was estimated to be 30%." To "Averaged over the period 2013-2015, the relative uncertainty of the inversion was estimated to be 30%."
RESPONSE: Corrected according to reviewer's suggestion (see manuscript with Track Changes).

Page 15, lines 458-460: change "In the same figures the differences between posterior and prior emissions (ECLIPSEv5) are shown (right panels) to indicate the biggest emission changes compared to the a priori dataset." to "The right panel of the same figures shows the differences between posterior and prior emissions (ECLIPSEv5) and highlights the biggest emission changes compared to the a priori dataset."
RESPONSE: Corrected according to reviewer's suggestion (see manuscript with Track Changes).

Page 16, line 464: change "... was seen in 60◦N- 135◦W" to "was located at 60◦N, 135◦ W".
RESPONSE: Corrected (see manuscript with Track Changes).

Page 16, lines 474-476: change “In this region four uranium mines are located that use diesel generators, diesel trucks, and likely also other diesel-powered machinery.” to “Uranium mines are located in this region. These mines use diesel generators, diesel trucks, and other diesel-powered machinery.”
RESPONSE: Corrected according to reviewer’s suggestion (see manuscript with Track Changes).

Page 18, lines 544-545: change “By separating the inversion domain into continental regions, it is easily seen where biomass burning is important.” to “Separating the inversion domain into continental regions reveals where biomass burning is important.”
RESPONSE: Corrected according to reviewer’s suggestion (see manuscript with Track Changes).

Page 18, line 550: change “. . . largest peak was already in April. . .” to “ . . .larges peak appears in April. . .”
RESPONSE: Corrected (see manuscript with Track Changes).

Page 19, line 563-565: change “We performed a sensitivity study to assess the best representative species for BC in terms of scavenging and removal and the best representative emission inventory to be used as the prior information for our inversion.” to “We performed a sensitivity study to assess the best representative species for BC according to the efficiency of in-cloud and below-cloud scavenging, and the best representative emission inventory to be used as the prior information for our inversion.”
RESPONSE: Corrected according to reviewer’s suggestion (see manuscript with Track Changes).

RESPONSES to comments of Anonymous Referee #2

This work by Evangeliou et al. performed a Bayesian inverse analysis of BC emission fluxes at northern high latitudes using ground-based observations and a Lagrangian particle model. The authors accounted for the uncertainties associated with BC wet removal with simulations using a range of scavenging parameters and prior emissions. The inversion found high BC emissions from gas flaring in Russia and Canada. The inversion also found that retrieved emission seasonality is different from that in emission inventory in N. America, N. Europe and N.Siberia. The topic is interesting and the paper is overall well organized but the method description still needs some clarification.
I support the publication of the paper if the following major comments are addressed.
RESPONSE: We would like to acknowledge reviewer's attempt to help improving this paper. We have tried to correct and answer his comments.

Major comments

The paper lacks sufficient description about the specification of error covariance matrices, B and R, which are useful for readers to evaluate the validity of the inversion method.
RESPONSE: The diagonal elements of B (the variances) are the squares of the uncertainties of each grid cell where the uncertainties are calculated as a fraction of the total prior emission estimate with a lower limit. For R, normally this is a diagonal matrix (it only has off-diagonal elements if one uses the calculation of aggregation error). The diagonal elements of R are calculated as the quadratic sum of the observation, aggregation and background uncertainties. In our case we had zero for the background uncertainty (zero background for BC).
Details and specifications of the error covariance matrices can be found in Thompson and Stohl (2014). Prior to publication of this manuscript in ACPD, we were asked many times to change the methodology of the manuscript, in order to pass the similarity test. Therefore, we were encouraged to omit many methodological details that can be found in the aforementioned paper.

Thompson, R. L. and Stohl, A.: FLEXINVERT: an atmospheric Bayesian inversion framework for determining surface fluxes of trace species using an optimized grid, Geosci. Model Dev., 7, 2223-2242, https://doi.org/10.5194/gmd-7-2223-2014, 2014.

How large is the observation errors and prior errors? Are they assumed to have any spatial/temporal correlations? Are model errors considered in R?
RESPONSE: As described in Thompson and Stohl (2014) paper the inversion code treats observation error in two ways. Either one can assign a constant observation error or take observation error directly from the continuous measurements. We have chosen the second option, because we think that observation errors that have been given by the instruments are far more realistic.
As described in the paper released for the ECLIPSE emissions by Klimont et al. (2017), there are different types of uncertainties in ECLIPSE that stem from the way that each calculation has been made. For example for residential combustion, there are uncertainties in assumptions about heat value of various biofuels. For emissions from waste burning large uncertainties are attributed to only scarce measurements and

difficulties in finding reliable data on waste collection, recycling, and disposal rates. Large uncertainties exist in fuel consumption, its allocation between uses and technologies, and emission factors. Several other sources of uncertainty are also mentioned in Klimont et al. (2017) paper. This makes impossible to estimate a fixed uncertainty of the prior. We have used a minimum and maximum error. Then the prior error is calculated as a fraction of the maximum value of each pixel and its 8 surrounding ones, and then sets ocean pixels to the minimum value (see previous comment and info in Thompson and Stohl, 2014).
Error covariance matrix B has spatial and temporal correlations (off-diagonal elements). About the model errors, these are represented by the ensemble of runs that we have performed. Each member of the ensemble has different scavenging settings, so the range of results from our ensemble represents the range due to the uncertainty in the scavenging settings, which in our case is the largest model error.

Klimont, Z., Kupiainen, K., Heyes, C., Purohit, P., Cofala, J., Rafaj, P., Borken-Kleefeld, J., and Schöpp, W.: Global anthropogenic emissions of particulate matter including black carbon, Atmos. Chem. Phys., 17, 8681-8723, https://doi.org/10.5194/acp-17-8681-2017, 2017.

Also, I find the method description a little confusion. In Line 191, the authors claim that they conduct "ensemble of inversions" and conduct "the inversion for BC represented by 12 different scavenging coefficients and for four different prior emission datasets. However, in Line 358, "the posterior emissions were calculated for the best performing species and best prior emission inventory". So, what are the results of "ensemble of inversions" used for? Are they used in Section 3.1 and 3.2 (The text of these two sections does not mention inversion. I assume that these are results from forward model simulations rather than inversion)? Or are they used for uncertainty estimation? If so, authors need to describe in the Method section how to compute the final uncertainty value from the ensemble inversions.
RESPONSE: We have changed "the posterior emissions were calculated for …" with "the posterior emissions are presented for …". We present the results of posterior BC emissions for the best representative species and the best prior dataset. We use all inversion BC emissions (using 12 BC species and 4 prior datasets) to calculate uncertainty, as stated in the next sentences clearly. Describing how the model ensemble was used is just 1-2 sentences and, given that it would stand as a separate section in the methodology, we have decided to simply mention it in the Abstract, in the last sentence of Introduction and describe it in section 3.3.

The authors show that different wet removal parameters have little impact on simulated BC, which is interesting. But the authors can provide more information for readers to better evaluate this conclusion. (1) how BC aging and its hydrophilic/hydrophobic state is considered in the model? What is the uncertainty associated with this process? (2) what is the size of emitted BC, whether the size changes during transport, and is the simulation sensitive to the assumption of BC size? (3) are there evidence to support that the choices of parameter in Table 2 is adequate? (Grythe 2017 tested a larger ranges of parameters).
RESPONSE: (1) This has been already explained well in Grythe et al. paper referring to FLEXPART model. The level of detail of aerosol removal schemes in Lagrangian models is a limiting factor due to the Lagrangian model framework. A main consideration within

this framework is that each transported computational particle is independent of others. Extensions of this concept to allow for non-linear chemistry exist or FLEXPART (Cassiani, 2013), but the reference version of FLEXPART is a purely linear transport model. Within such a linear model, it is impossible to include aerosol processes, which depend on the aerosol concentration (e.g., coagulation or non-linear chemical reactions). Furthermore, to facilitate consistency between forward and backward runs of FLEXPART, parameterizations that depend on the age of the aerosol (i.e. time after emission for primary aerosols) should be avoided as well. This limits the level of sophistication that can be incorporated into an aerosol removal scheme. Nevertheless, a realistic treatment of aerosols is possible even with these limitations.
In other words, the aerosol ageing processes are not readily included in FLEXPART and the constant removal parameters cannot account for this transformation. However, this may not cause significant uncertainties as there are several observations that prove that BC is transformed very quickly into particles with aged, hydrophylic characteristics (e.g. Wittbom et al., 2014).
(2) In section 2.2 we state that we have used a logarithmic size distribution with an aerodynamic mean diameter of 0.25 μm, a logarithmic standard deviation of 0.3 and a particle density of 1500 kg m−3. We also give a reference (Long et al., 2013). The reference explains very well the morphology and size of BC particles emitted in different steps (initial, after agglomeration, etc.). The change of the size during transport is accounted for using the logarithmic size distribution. Of course the simulation is sensitive to the size of particles, since changing the size distribution would also change the residence times of BC particles. However, we only examined the sensitivity to the new scavenging scheme that is used in FLEXPART and not to different particle sizes.
(3) The selection of parameters in Table 2 was done according to Grythe et al. (2017) paper. Like the reviewer says, Grythe et al. used a larger range of parameters. In our paper, when changing scavenging parameters of BC, except for conducting a sensitivity analysis and estimate uncertainties, our top priority was to select the best representative species for BC, hence scavenging coefficients should be realistic. Of course, if we change these parameters drastically (like in Grythe et al. paper), the variability of the posterior concentrations will increase. Though, this has been already done in Grythe et al. paper and, besides, we would not have realistic values anymore.

Cassiani, M.: The volumetric particle approach for concentration fluctuations and chemical reactions in Lagrangian particle and particle-grid models, Bound.-Lay. Meterol., 146, 207–233, 2013.
Wittbom, C., Eriksson, A. C., Rissler, J., Carlsson, J. E., Roldin, P., Nordin, E. Z., Nilsson, P. T., Swietlicki, E., Pagels, J. H., and Svenningsson, B.: Cloud droplet activity changes of soot aerosol upon smog chamber ageing, Atmos. Chem. Phys., 14, 9831–9854, doi:10.5194/acp-14-9831-2014, 2014.
Long, C. M., Nascarella, M. A. and Valberg, P. A.: Carbon black vs. black carbon and other airborne materials containing elemental carbon: Physical and chemical distinctions, Environ. Pollut., 181, 271–286, doi:10.1016/j.envpol.2013.06.009, 2013.

The uncertainty estimates do not account for model transport errors and instrument errors. Section 2.2 and Figure 1 (g)-(i) show that the footprint varies greatly spatially. One may wonder how does this affect the inversion uncertainty? Can transport errors be more important than the choice of prior emission inventory and scavenging parameters in some regions distant from surface sites? Are observations informative for these

regions? One of the major finding is gas flaring emissions from Russia but Figure 1 (g)-(i) show small footprint in these regions. Also, Figure 12 shows that locations of intensive gas flaring are shifted from prior inventory but Figure 1 (d)-(f) shows the inversion grid there is very coarse. It is worthwhile to check the posterior error covariance matrix to see how confident the inversion is about the conclusions?
RESPONSE: Model transport errors are not explicitly accounted for, but they are likely small compared to the error in the scavenging. We account for the scavenging error by running ensembles. And using e.g. inter-quartile range or SD over the ensemble to estimate your posterior uncertainty, then that already answers the question about how this affects the inversion uncertainty. As regards to the instrument errors, if the reviewer talks about measurements of BC, then these errors are included in the inversion. Each continuous measurement site gives concentrations plus measurement errors (see also previous comment).
Returning to scavenging errors, they are much more important that transport errors. This has been proved in Thompson et al. (2017) for the CH4 inversion in high northern latitudes. There, GFS versus ECMWF meteorology are compared as a proxy for transport error and is found transport error to be relatively small in most cases (note this does not calculate the true transport error but gives some indication). In the attached figure R2_F1, we show the error (in concentration units) calculated from all runs with different scavenging parameters for year 2013.
To answer the question about whether the observations are informative for remote sites, we can simply look at the footprints of Fig.1 in the manuscript for these observations. There, we can observe problems in 2014 in N. America due to the lack of measurements (already discussed in the paper) and over areas between Finland and Tiksi station (also discussed in the paper) for all years due to the same reason (lack of measurements).

Thompson, R. L., Sasakawa, M., Machida, T., Aalto, T., Worthy, D., Lavric, J. V., Lund Myhre, C., and Stohl, A.: Methane fluxes in the high northern latitudes for 2005–2013 estimated using a Bayesian atmospheric inversion, Atmos. Chem. Phys., 17, 3553-3572, https://doi.org/10.5194/acp-17-3553-2017, 2017

Minor comments Abstract.
The writing of the abstract can be improved. Line 17-19 and 23-25 seem to be out of place.
RESPONSE: Corrected. The first sentence (L17-19) was transferred to the next paragraph where the main results are summarized and the second one (L23-25), which is rather methodology-related, was transferred to the first paragraph (see manuscript with Track Changes).

Line 37: main of atmospheric particular matter (?)
RESPONSE: Obviously a word is missing here, so we have corrected the sentence to: "Light absorbing species, such as black carbon (BC), are the main components of atmospheric particulate matter, affecting air quality, weather and climate." Please see manuscript with Track Changes.

Line 39: gas flaring is open high- temperature combustion of natural gas in the oil/gas field. This source may be worth mentioning here because relevance to the results.

RESPONSE: We agree that it is a very good idea to also include this source due to its relevance with the results. Please see section 1. Introduction in the manuscript with Track Changes.

Line 80: maybe worthwhile to compare the results with this emission dataset?
RESPONSE: The emissions dataset used in Popovicheva et al. paper is ECLIPSEv5 with GFED4, exactly the same with the ones used with the Bayesian inversion in the current paper.

Line 152: the removal efficiency depends on BC aging (hydrophilic/hydrophobic) and size. How are they treated in the particle model?
RESPONSE: See also previous comment on aging. Aerosol ageing processes are not readily included in FLEXPART and the constant removal parameters cannot account for this transformation. However, this may not cause significant uncertainties as there are several observations that prove that BC is transformed very quickly into particles with aged, hydrophylic characteristics (e.g. Wittbom et al., 2014).

Wittbom, C., Eriksson, A. C., Rissler, J., Carlsson, J. E., Roldin, P., Nordin, E. Z., Nilsson, P. T., Swietlicki, E., Pagels, J. H., and Svenningsson, B.: Cloud droplet activity changes of soot aerosol upon smog chamber ageing, Atmos. Chem. Phys., 14, 9831–9854, doi:10.5194/acp-14-9831-2014, 2014.

Line 363-366: not clear how these uncertainties are individually computed and then combined. Equations are useful here. And it may also be a good idea to move the description in Method sections.
RESPONSE: We have clarified this now in section 3.3. Usually, one can combine two uncertainties from different processes by propagation and there are different methods to do this (see for example: http://lectureonline.cl.msu.edu/~mmp/labs/error/e2.htm).

Line 467-469: This type of uncertainty is not included in current uncertainty estimation but should be available by analyzing posterior error covariance matrix if B and R are properly assigned.
RESPONSE: Since we used an ensemble to calculate the posterior uncertainty, and take also into account the uncertainty due to scavenging, we do not have the error correlations. However, we can see the uncertainty for each grid cell in Whitehorse that is shown to be very high in 2013 and 2015, but not in 2014 (Fig.S5). If we also check the total footprint for all stations in 2014 (Fig. 1), we can easily understand that the coverage for this region is very poor. And this poor coverage is just due to the lack of measurements in this particular year, as we state in the manuscript.

Section 4.4: The inversed emission seasonality is very interesting. I'd suggest summarizing the major finding about the seasonality in the abstract.
RESPONSE: Corrected! A sentence with the most important findings was introduced in Abstract (see manuscript with Track Changes).

Line 553-555: what type of errors in the inversion?
RESPONSE: We agree with the reviewer. We do not really know what types of errors we have here. We have removed this comment. Please see last paragraph of section 4.4 in manuscript with Track Changes.

Table 3: “four different optimized emission estimates are given”? Are they prior or posterior emissions? I am confused.
RESPONSE: We acknowledge the reviewer for pointing out this typo error. We have corrected the legend.
In this Table, we present annual posterior emissions of BC for N. America, N. Europe, N. Siberia and the 2 flaring regions in Russia. They are highlighted as “Posterior (ECLIPSEv5)”, because they were calculated using best representative species and best prior inventory. For comparison, we give the respective emissions for the same 5 regions in the four prior datasets highlighted as “ACCMIPv5 (prior)”, “EDGAR_HTAPv2.2 (prior)”, “MACCity (prior)” and “ECLIPSEv5 (prior)”.

Figure 1: It’s impossible to read labels in panels (a)-(c). It may be a good idea to use the projection in Figure 6 for reader to compare different figures easily.
RESPONSE: The real goal of (a) – (c) panels there is to just show the density of the measurement stations that were used each year. All the characteristics, locations and instrument types can be seen in Table 1. Switching the projection to Mercator as suggested by the reviewer does not improve or solve the problem (see attached Figure R2_F2), so we would like to keep the current projection, which is consistent with the rest of the panels in Fig. 1

Figure 2: Use a consistent projection for panels (a)-(g) and Figure 6 so readers can compare easily.
RESPONSE: We see the point of the reviewer, although that’s the main reason that we also present the difference between posterior and prior emissions in Figure 6; so the readers can compare easily.
We have corrected Figure 2 as suggested, although we doubt that one will be able to distinguish different source locations on such a complex Figure.

Figure 3 and 4: Two figures provide very similar information. Consider removing one.
RESPONSE: These 2 different pictures are used for different reasons in the text. They also use 2 different statistics and having 2 statistics is always better that having only one. Since there are no space limitations in ACP, we would prefer to keep both of them as an additional evidence of our findings within the text.

Figure 7 - 9: These evaluations are quite interesting. But since the inversion is done with ECLIPSEv5, it is a fair comparison between posterior emissions with averaged RMSE from four emission inventories. RMSEpri from ECLIPSEv5 should be listed as well.
RESPONSE: Corrected!! We have introduced RMSE values for ECLIPSE as well, as suggested by the reviewer.

Figure 9: The difference between posterior and ECLIPSEv5 is very small, which may be indicative that the observations are not informative to emissions in this region. See major comments for uncertainty estimations.
RESPONSE: We agree with the reviewer that lack of observations there constrains sources poorly in areas between Finland up to Tiksi station pushing the inversion towards prior emissions. However, there is no solution for this.

Figure 11-12: “Black rectangles show vegetation fires adopted from Hao et al.” Choose another color. Black color is already used for map borders. Also, they are better referred to as dots rather than rectangles.
RESPONSE: Corrected! We have introduced dark green points to represent fire spots. See Track Changes manuscript.

Figure 13: The prior emissions plotted in panel d (N.Siberia) of Figure 13 seems to be wrong as they are much lower than the annual total emissions reported in Table 3.
RESPONSE: Again, thanks a lot for pointing out this mistake. We had accidentally plotted another area, where N. Siberia should be. We have now corrected it! Please see Track Changes.

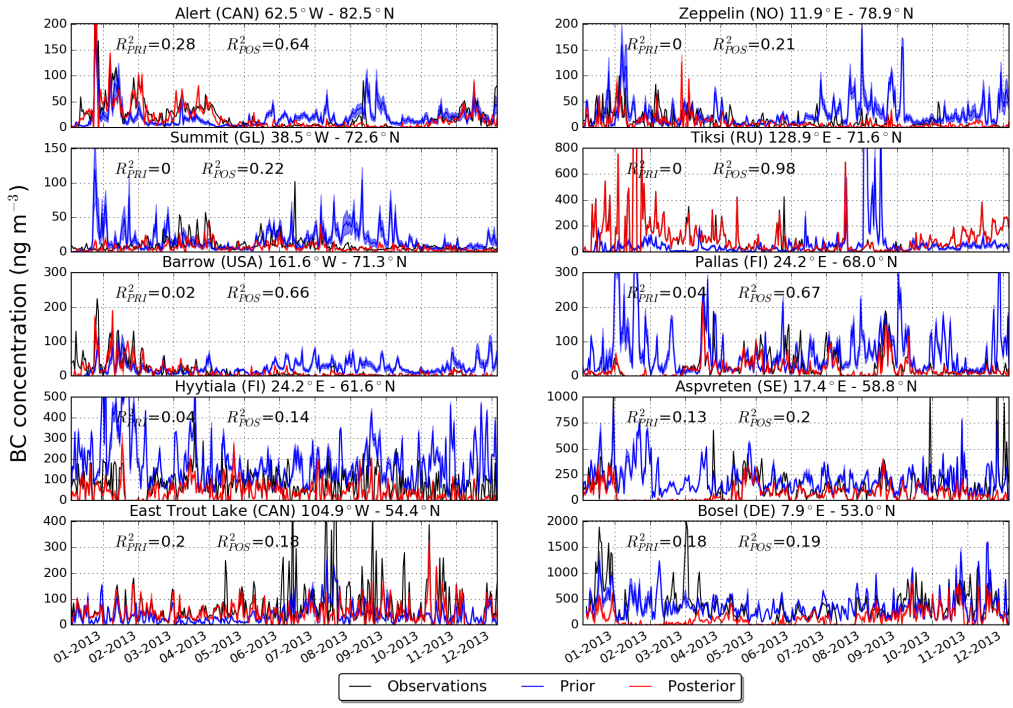


FIGURE R2_F1

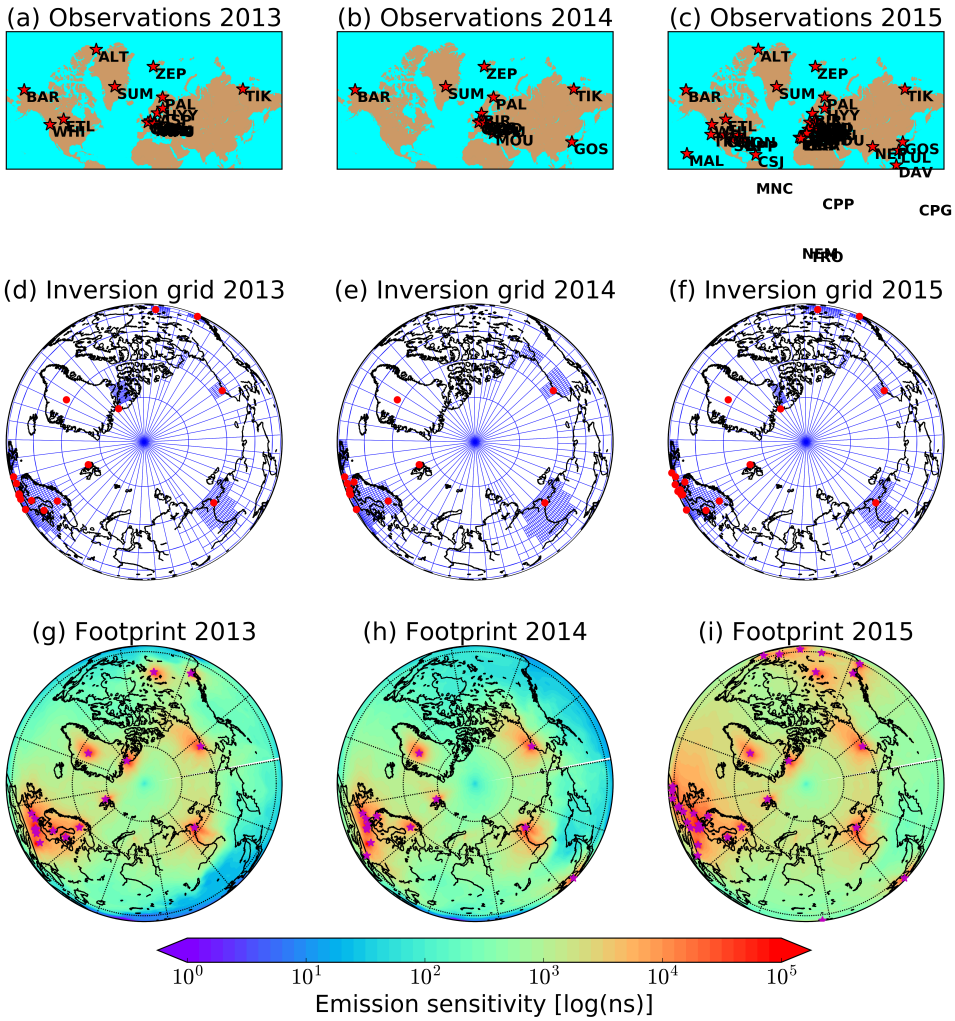
(a) Observations 2013
(b) Observations 2014
(c) Observations 2015
ALT
ZEP
BAR
SUM
PAL
TIK
WHI
MOU
GOS
MAL
CSJ
MNC
CPP
CPG
DAV
(d) Inversion grid 2013
(e) Inversion grid 2014
(f) Inversion grid 2015
(g) Footprint 2013
(h) Footprint 2014
(i) Footprint 2015
$10^0$
$10^1$
$10^2$
$10^3$
$10^4$
$10^5$
Emission sensitivity [log(ns)]

FIGURE R2_F2

# Top–down estimates of black carbon emissions at high latitudes using an atmospheric transport model and a Bayesian inversion framework

**Nikolaos Evangeliou *, Rona L. Thompson, Sabine Eckhardt, Andreas Stohl**

Norwegian Institute for Air Research (NILU), Department of Atmospheric and Climate Research (ATMOS), Kjeller, Norway.

* Correspondence to: N. Evangeliou (nikolaos.evangeliou@nilu.no)

## Abstract

This paper presents the results of BC inversions at high northern latitudes (>50°N) for the 2013–2015 period. A sensitivity analysis was performed to select the best representative species for BC and the best a priori emission dataset. The same model ensemble was used to assess the uncertainty of the a posteriori emissions of BC due to scavenging and removal and due to the use of different a priori emission inventory. A posteriori concentrations of BC simulated over Arctic regions were compared with independent observations from flight and ship campaigns showing, in all cases, smaller bias, which in turn witnesses the success of the inversion. The annual a posteriori emissions of BC at latitudes above 50°N were estimated as 560±171 kt $yr^{-1}$, significantly smaller than in ECLIPSEv5 (745 kt $yr^{-1}$), which was used and the a priori information in the inversions of BC. The average relative uncertainty of the inversions was estimated to be 30%.

A posteriori emissions of BC in North America are driven by anthropogenic sources, while biomass burning appeared to be less significant as it is also confirmed by satellite products. In North Europe, a posteriori emissions were estimated to be half compared to the a priori ones, with the highest releases to be in megacities and due to biomass burning in Eastern Europe. The largest emissions of BC in Siberia were calculated along the transect between Yekaterinsburg and Chelyabinsk. The optimised emissions of BC were high close to the gas flaring regions in Russia and in Western Canada (Alberta), where numerous power and oil/gas production industries operate. Flaring emissions in Nenets-Komi oblast (Russia) were estimated to be much lower than in the a priori emissions, while in Khanty-Mansiysk (Russia) they remained the same after the inversions of BC. Increased emissions in the borders between Russia and Mongolia are probably due to biomass burning in villages along the Trans-Siberian Railway. The maximum BC emissions in high northern latitudes (>50°N) were calculated for summer months due to biomass burning and they are controlled by seasonal variations in Europe and Asia, while North America showed a much smaller variability.


Nikolaos Evangeliou 21/9/2018 14:37
**Deleted:** prior

Nikolaos Evangeliou 21/9/2018 14:36
**Deleted:** posterior

Nikolaos Evangeliou 21/9/2018 14:38
**Deleted:** prior

Nikolaos Evangeliou 24/9/2018 11:18
**Moved down [1]:** The optimised emissions of BC were high close to the gas flaring regions in Russia and in Western Canada (Alberta), where numerous power and oil/gas production industries operate.

Nikolaos Evangeliou 21/9/2018 14:36
**Deleted:** posterior

Nikolaos Evangeliou 21/9/2018 14:38
**Deleted:** prior

Nikolaos Evangeliou 21/9/2018 14:37
**Deleted:** Posterior concentrations of BC simulated over Arctic regions were compared with independent observations from flight and ship campaigns showing, in all cases, smaller bias, which in turn witnesses the success of the inversion.

Nikolaos Evangeliou 21/9/2018 14:37
**Deleted:** Posterior

Nikolaos Evangeliou 21/9/2018 14:37
**Deleted:** posterior

Nikolaos Evangeliou 21/9/2018 14:38
**Deleted:** prior

Nikolaos Evangeliou 24/9/2018 11:18
**Moved (insertion) [1]**

Nikolaos Evangeliou 21/9/2018 14:38
**Deleted:** prior

## 1 Introduction

Light absorbing species, such as black carbon (BC), are the main components of atmospheric particulate matter, affecting air quality, weather and climate. BC originates from the incomplete combustion of fossil fuels (primarily coal and diesel), from open high–temperature combustion of natural gas in the oil/gas field (gas flaring), as well as from the burning of biomass and biofuels. BC particles affect cloud formation and precipitation as they act as cloud condensation nuclei in their hydrophilic form (Wang et al., 2016). BC is also a major driver of climate change contributing to global warming with a radiative forcing at the top of the atmosphere ranging between 0.17 and 0.71 W $m^{-2}$ (Bond et al., 2013; Myhre et al., 2013; Wang et al., 2014). BC deposited in Arctic snow surfaces in concentrations of up to 30 ng $g^{-1}$ can reduce snow albedo by 1–3% (Hegg et al., 2009) in fresh snow and up to 3 times more as snow ages and the BC particles become more concentrated (Clarke and Noone, 1985). Airborne BC also warms the air and reduces tropical cloudiness by absorbing the incoming solar radiation (Ackerman, 2000). It also reduces atmospheric visibility and increases aerosol optical depth (Jinhuan and Liquan, 2000). From a health perspective, BC particles, generally being sub-micron in size, can penetrate into the lungs and cause pulmonary diseases (e.g., Wang et al., 2014).

To improve understanding about how BC affects climate and to develop effective policies to tackle BC's associated environmental problems requires accurate knowledge of the emissions and their spatiotemporal distribution. Most commonly, BC emission inventory datasets are built by "bottom up" approaches, which are based on activity data and emission factors and proxy information for spatial disaggregation, but these methods are considered to have large uncertainties (Cao et al., 2006). Numerous global or regional emission inventories of BC have been constructed previously (Bond et al., 2004; Schaap et al., 2004; Streets et al., 2003); nevertheless, emission uncertainties contribute significantly to the overall uncertainty of modelled concentrations of BC. Emission uncertainties affect even more significantly regional/episodic simulations, as in many cases emissions deviate from the annual mean. Such studies represent a useful tool to improve our understanding of the relationship between observed concentrations of BC and BC emissions. Furthermore, BC emissions have their most pronounced effect on the regional scale due to the relatively short atmospheric lifetime of BC (Hodnebrog et al., 2014; Samset et al., 2014),.

The relative differences between different emission inventories are largest for the high latitudes (AMAP, 2015) and particularly in high-latitude Russia where emission information is poor. For this area, a new satellite-based high-resolution inventory showed that BC

Nikolaos Evangeliou 24/9/2018 11:25
**Deleted:** components,

Nikolaos Evangeliou 24/9/2018 11:23
**Deleted:** is

emissions from Biomass Burning (BB) might have been 3.5 times higher than emissions given in the Global Fire Emissions Database (GFEDv4) (Hao et al., 2016), if more realistic emission factors are used (May et al., 2014). Furthermore, new sources of BC in the same area have been identified recently. For example, emissions from gas flaring by the oil industry have been missing from most emission inventories and may be an important source of BC at high latitudes (Stohl et al., 2013). For instance, in 2008 Russia was responsible for nearly one third of the gas flared globally (Elvidge et al., 2009). However, the gas flaring source is highly uncertain. For example, based on isotopic measurements, Winiger et al. (2017) reported recently that the contribution from gas flaring to BC measured at Tiksi in Siberia is lower than estimated by Stohl et al. (2013), while recently published bottom-up inventories (Huang et al., 2015; Huang and Fu, 2016) suggested even higher gas flaring emissions. Finally, Popovicheva et al. (2017) reported that one existing emission dataset of BC captured surface concentrations in the Russian Arctic quite efficiently.

In this study, we estimated the BC emissions at high northern latitudes using atmospheric observations of BC in a Bayesian inversion framework. Emissions were estimated for the region north of 50°N because this is the region with the largest influence on Arctic surface concentrations (Klonecki, 2003; Stohl, 2006). We determine the emissions with monthly time resolution for the years 2013, 2014 and 2015. We first describe the observation data, the transport model and the Bayesian inversion technique used, as well as the prior emission information. We then assess the sensitivity of the transport model to different scavenging coefficients (below-cloud and in-cloud) for BC and to different emission inventories. We finally present optimised BC emissions, discuss these results in comparison with independent estimates and calculate the uncertainty of the inversions with respect to different scavenging parameters used for BC and using four different prior emission datasets.

## 2 Methodology

### 2.1 Observation network

Atmospheric observations of BC were retrieved from the World Data Centre for Aerosols (http://ebas.nilu.no) and from the International Arctic Systems For Observing The Atmosphere (http://www.esrl.noaa.gov/psd/iasoa/). An overview of the stations used in this paper can be found in Table 1 and Figure 1a–c. The selected measurements were performed with different types of instruments that may differ substantially. When measurements are

Nikolaos Evangeliou 27/9/2018 11:26
**Deleted:** Table 1

Nikolaos Evangeliou 27/9/2018 11:26
**Deleted:** Figure 1

based on light absorption we refer to Equivalent BC (EBC), while measurements based on thermal-optical methods refer to elemental carbon (EC) (Petzold et al., 2013).

At Alert (ALT), Appalachian (APP), Asprveten (ASP), Birkenes (BIR), East Trout Lake (ETL), South Great Planes (SGP), Steamboat Springs (COL), Trinidad Head (TRI) and Whistler (WHI) measurements were performed with particle soot absorption photometers (PSAPs). At Annaberg-Buchholz (ANB), Bösel (BOS), Cabauw Zijdeweg (CAB), Hyytiälä (HYY), Leipzig (LEI), Melpitz (MEL), Nepal Climate Observatory (NEP), Pallas (PAL), Ústí n.L.-mesto (ULM) and Waldhof (WLD) the particle light absorption coefficient was measured by multi-angle absorption photometers (MAAP; Petzold and Schönlinner, 2004), which are in excellent agreement with other particle light absorption photometers such as a photoacoustic sensor (e.g., Muller et al., 2011). In the MAAP instrument, particles are continuously sampled on filter tape, with loaded spots subsequently analysed by Raman spectroscopy to derive the particle mass concentration of soot (Nordmann et al., 2013). The cut-off sizes of the different MAAP instruments varied between 1 and 10 μm. Continuous light absorption photometers (CLAP, Model PSAP; 565 nm) were used at Barrow (BAR), Bondville (BON), Gosan (GOS), K-puszta (KPU), BEO Moussala (MOU) and Summit (SUM). Although these instruments were calibrated to measure the aerosol absorption coefficient, a previous study at this site revealed that a value of 10 $m^2$ $g^{-1}$ is a reasonable conversion factor to determine the BC concentration (Gelencsér et al., 2000). Aethalometers were used at Tiksi (TIK) and Zeppelin (ZEP).

All these stations measure the particle light absorption coefficients of different size fractions of the aerosol at wavelengths around 530–550 nm. Then the light absorption coefficients are converted to EBC mass concentrations under certain assumptions (Petzold et al., 2013). This is done externally for instruments such as MAAP, CLAP, PSAP etc. using a mass absorption efficiency of 10 $m^2$ $g^{-1}$ (Bond and Bergstrom, 2006). For aethalometers, the conversion is done internally by the instrument. All station measurements are routinely filtered to remove influence from local sources.

### 2.2 Source – Receptor Relationships (SRRs)

We used the Lagrangian Particle Dispersion Model (LPDM), FLEXible PARTicle dispersion model (FLEXPART) (Stohl et al., 1998, 2005) to model atmospheric transport. Using LPDMs to model particle or trace gas concentrations has several advantages over Eulerian models, namely they can have quasi-infinite resolution and they are not subject to numerical diffusion. Thus they can provide better resolved source-receptor relationship (SRR)

fields, which describe the relationship between the sensitivity of a "receptor" to a "source" element, as described by Seibert and Frank (2004). SRRs for the lowest model level are often called footprint emission sensitivities or even just footprints.

SRRs were calculated using FLEXPART version 10 in a backwards mode (see Stohl et al., 2005) in which computational particles are released backward in time from the observation sites (receptors). When the number of observation sites is smaller than the number of unknown flux grid cells this mode is computationally more efficient than forward calculations. Furthermore, backward simulations can be initiated exactly at the measurement point without initial diffusion of information into a grid cell. This important advantage of LPDMs also facilitates high spatial resolution of the model output around the measurement sites. As meteorological input data, European Centre for Medium-Range Weather Forecasts operational meteorological analyses were used with 137 vertical levels and a horizontal resolution of 0.5°×0.5°. Retroplumes were calculated at hourly intervals at each of the receptors. 40,000 particles for each retroplume were released and followed 30 days backwards in time. This should be a sufficiently long time in order to include almost all contributions to BC concentration at the receptor given the atmospheric lifetime of BC (in the range of 2–10 days, Benkovitz et al., 2004; Koch and Hansen, 2005; Park et al., 2005; Textor et al., 2006).

The treatment of scavenging is a major uncertainty for modelling BC (Browse et al., 2012). Therefore, an ensemble of 12 model simulations was performed each with different BC tracers having different in–cloud and below–cloud scavenging properties (Table 2). This method allows the sensitivity of the SRRs (produced by FLEXPART) to scavenging to be quantified. Table 2 shows the different below–cloud and in–cloud scavenging parameters used within the model in the sensitivity runs. For all tracers, we assumed a logarithmic size distribution with an aerodynamic mean diameter of 0.25 μm, a logarithmic standard deviation of 0.3 and a particle density of 1500 kg $m^{-3}$ (Long et al., 2013). The dry deposition scheme in FLEXPART is based on the resistance analogy (Slinn 1982). The present version of the model uses the precipitation rate from ECMWF to determine below-cloud scavenging and the cloud liquid water and ice content, precipitation rate and cloud depth from ECMWF to calculate in-cloud scavenging (see Grythe et al., 2017).

The SRR at the lowest model layer (in seconds) (Figure 1g–i) can be multiplied with gridded emission fluxes from a BC emission inventory (in kg $m^{-2}$ $s^{-1}$) distributed over the layer depth (100 m). This gives the prior concentration of BC at the receptor point (in ng $m^{-3}$).

Nikolaos Evangeliou 27/9/2018 11:26
**Deleted:** Table 2

Nikolaos Evangeliou 27/9/2018 11:26
**Deleted:** Table 2

Nikolaos Evangeliou 27/9/2018 11:26
**Deleted:** Figure 1

## 2.3 Bayesian inversion

The inversion methodology used in the present study, FLEXINVERT, is described fully in Thompson and Stohl (2014) and has been already used in studies of $CH_4$, HFC-125, HFC-134a and $SF_6$ (Brunner et al., 2017; Thompson et al., 2015, 2017). Since atmospheric transport and deposition are linear operations, they can be described as a Jacobian matrix of SRRs ($\mathbf{H}$). The BC concentrations ($\boldsymbol{y}$) can then be modelled given an estimate of the emissions ($\boldsymbol{x}$) as follows:

$$\boldsymbol{y} = \mathbf{H}(\boldsymbol{x}) + \boldsymbol{\varepsilon} \qquad (1)$$

where $\boldsymbol{\varepsilon}$ is an error associated with model representation, such as the modelled transport and deposition as well as the measurements. Since $\mathbf{H}$ is generally not invertible (or may have no unique inverse), statistical optimization methods are used, which require prior information for regularization. According to Bayesian statistics, the problem can be expressed as the maximization of the probability density function of the emissions given the prior information and observations and is equivalent to finding the minimum of the cost function:

$$\mathbf{J}(\boldsymbol{x}) = \frac{1}{2}(\boldsymbol{x} - \boldsymbol{x_b})^T \mathbf{B^{-1}} (\boldsymbol{x} - \boldsymbol{x_b}) + \frac{1}{2}(\boldsymbol{y} - \mathbf{H}\boldsymbol{x})^T \mathbf{R^{-1}} (\boldsymbol{y} - \mathbf{H}\boldsymbol{x}) \qquad (2)$$

where $\mathbf{B}$ and $\mathbf{R}$ are the error covariance matrices for the prior emissions and the observations, respectively. The error in the observation space also accounts for model representation errors that are not related to the BC emissions. The emissions that minimize the cost function can be found by solving the first order derivative of equation (2). Hence, the following equation can be derived for the most probable emissions, $\boldsymbol{x}$ (for details see e.g. Tarantola, 2005):

$$\boldsymbol{x} = \boldsymbol{x_b} + \mathbf{B}\mathbf{H^T}(\mathbf{H}\mathbf{B}\mathbf{H^T} + \mathbf{R})^{-1}(\boldsymbol{y} - \mathbf{H}\boldsymbol{x_b}) \qquad (3)$$

In this study, the state vector contains the monthly unknown surface emissions on the grid of variable resolution (Figure 1d–f) and has a resolution of between 1.0°×1.0° and 8.0°×8.0°. The total number of emission variables to be determined was 1422 for 2013, 1404 for 2014 and 1436 for 2015. The posterior error covariance matrix, $\mathbf{A}$, is equivalent to the inverse of the second derivative of the cost function. However, to account for the uncertainty in the scavenging parameters and different prior information, we instead conduct ensemble of inversions to estimate the posterior uncertainty in order to account for the systematic errors. To do this, we conduct the inversion for BC represented by 12 different scavenging coefficients (see Table 2) and for four different prior emission datasets, and do this for each of the three years of our study (2013–2015). The resulting model ensemble (12×4=48) for each year defines the posterior uncertainty due to scavenging and use of different a priori information (section 3.3).

Nikolaos Evangeliou 27/9/2018 11:26
**Deleted:** Figure 1

Nikolaos Evangeliou 27/9/2018 11:26
**Deleted:** Table 2

Since negative values for the posterior emissions are mathematically possible but physically unlikely, we applied a subsequent inequality constraint on the emissions following the method of Thacker (2007). This is a truncated Gaussian approach in which inequality constraints are applied as error-free "observations":

$$\hat{\boldsymbol{x}} = \boldsymbol{x} + \mathbf{A}\mathbf{P}^{\mathbf{T}}(\mathbf{P}\mathbf{A}\mathbf{P}^{\mathbf{T}})^{-\mathbf{1}}(\boldsymbol{c} - \mathbf{P}\boldsymbol{x}) \qquad (4)$$

where **A** is the posterior error covariance matrix, **P** is a matrix operator to select the variables that violate the inequality constraint, and $\boldsymbol{c}$ is a vector of the inequality constraint, which in this case is zero.

The emissions were solved on an irregular grid, which has been optimized based on the SRRs to give higher resolution (1.0° × 1.0°) in regions where there is strong contribution from emission sources to BC concentrations and lower (8.0° × 8.0°) where there is a weak contribution (Stohl et al., 2009). Then, the results are interpolated onto a uniform grid of 1.0°×1.0° resolution from 180°W to 180°E and 50°N to 90°N and are given at monthly time resolution for 2013, 2014 and 2015. To constrain emissions of BC monthly, a temporal correlation scale length between flux time-steps equal to 90 days was set.

## 2.4 A priori emission information

In the present study, the emission inventories ECLIPSE (Evaluating the CLimate and Air Quality ImPacts of ShortlivEd Pollutants) version 5 (Klimont et al., 2017) (available here: http://www.iiasa.ac.at/web/home/research/researchPrograms/air/Global_emissions.html), EDGAR (Emissions Database for Global Atmospheric Research) version HTAP_V2.2 (Janssens-Maenhout et al., 2015) (available here: http://edgar.jrc.ec.europa.eu/methodology.php#), ACCMIP (Emissions for Atmospheric Chemistry and Climate Model Intercomparison Project) version 5 (Lamarque et al., 2013) (available here: http://accent.aero.jussieu.fr/ACCMIP_metadata.php) and MACCity (Monitoring Atmospheric Composition & Climate / megaCITY - Zoom for the ENvironment) (Wang et al., 2014) (available here: http://accent.aero.jussieu.fr/MACC_metadata.php) were used as the prior emission estimates of BC (see Figure 2).

The ECLIPSE emission inventory (Figure 2a) accounts for waste burning, industrial combustion and processing, surface transportation that also includes power plants, energy conversion and extraction that also includes gas flaring, residential and commercial combustion.

The HTAP_V2 dataset (Figure 2b) consists of high-resolution gridded emissions of BC based on nationally reported emissions combined with regional scientific inventories. It

Nikolaos Evangeliou 27/9/2018 11:26
**Deleted:** Figure 2

Nikolaos Evangeliou 27/9/2018 11:26
**Deleted:** Figure 2

Nikolaos Evangeliou 27/9/2018 11:26
**Deleted:** Figure 2

includes the sources of aviation, inland waterways and marine shipping, energy production other than electricity generation, industrial processes, solvent production and application, electricity generation, ground transport, buildings heating, cooling, equipment, and waste disposal or incineration.

The ACCMIP simulations use the BC emission inventory covering the historical period (1850–2000) provided by (Lamarque et al., 2010), which is built for the climate model simulations in CMIP5 (Figure 2c). Anthropogenic emissions are mainly based on Bond et al. (2004) but apply new emission factors. The year 2000 dataset was used for harmonization with the future emissions determined by Integrated Assessment Models (IAMs) for the four Representative Concentration Pathways (RCP4.5, RCP6, and RCP8.5). They include emissions from energy production and distribution, industry (combustion and non-combustion), transportation, maritime transport and aviation, residential and commercial combustion and solvent extraction, agricultural production and waste treatment.

MACCity (Figure 2d) was built as an extension of the historical emissions dataset of ACCMIP. It provides monthly averaged sectorial emissions for each year during the 1960-2010 period. This dataset was based on the decadal ACCMIP emissions for 1960-2000 and the 2005 and 2010 emissions provided by RCP 8.5. This scenario was chosen since it included some information on recent emissions at the regional scale in Europe and North America. The emission sectors are consistent with Lamarque et al. (2010).

Emissions from biomass burning were adopted from the Global Fire Emissions Database, Version 4 (GFEDv4) (Giglio et al., 2013) and implemented to each of the four emission inventories for 2013, 2014 and 2015. Emissions from gas flaring are only included in ECLIPSEv5 inventory.

# 3 Results

## 3.1 Sensitivity to scavenging and selection of the best representative species for BC

The comparison of the simulated and observed concentrations for the 12 different BC tracers (see Table 2) is shown in Taylor diagrams in Figure 3 for ECLIPSEv5 and in Figure S 1 for ACCMIPv5, EDGAR_HTAPv2.2 and MACCity, only for those stations that had continuous measurements for all the years of our study (2013–2015) namely ZEP, SUM, TIK, BAR, PAL, CAB, MEL and LEI (see Table 1). For all the different BC species,

Nikolaos Evangeliou 27/9/2018 11:26
**Deleted:** Figure 2

Nikolaos Evangeliou 27/9/2018 11:26
**Deleted:** Figure 2

Nikolaos Evangeliou 27/9/2018 11:26
**Deleted:** Table 2

Nikolaos Evangeliou 27/9/2018 11:26
**Deleted:** Figure 3

Nikolaos Evangeliou 27/9/2018 11:26
**Deleted:** Figure S 1

Nikolaos Evangeliou 27/9/2018 11:26
**Deleted:** Table 1

concentrations of BC were calculated using the FLEXPART SRR and the four different emission datasets for 2013, 2014 and 2015.

Correlations of modelled and observed surface concentrations of BC were high (>0.5) only at stations ALT, MEL and LEI that present low normalised standard deviation (NSD) values (<1) and low normalised root mean square error (nRMSE) values. All NSD values were below 1.5 except at TIK and ULM stations (see Figure 3 and Figure S 1). In general, dispersion models fail to reproduce BC concentrations close to TIK station (Eckhardt et al., 2015; Evangeliou et al., 2016), as the station has been reported to receive pollution from local anthropogenic sources (Asmi et al., 2016). ULM station is located on the border between Germany and the Czech Republic and was shown previously to be strongly affected by BC emissions from residential combustion sources (Schladitz et al., 2015). The model-observation mismatches ($[model - observations]/observations$) due to the use of 12 different species for BC can be seen in Figure S 2 for the years 2013, 2014 and 2015. These values are average concentrations from the use of the four different emissions inventories (ECLIPSEv5, ACCMIPv5, EDGAR_HTAPv2.2 and MACCity). The extreme perturbation of the scavenging coefficients of BC caused an average relative model-observation mismatch (normalised against observations) of about 39% in 2013 (Figure S 2) at all stations.

Similar to 2013, 12 species with different scavenging parameters were used for BC following Table 2 in 2014 and the comparison with observations is shown in Taylor diagrams in Figure 3 using ECLIPSEv5 emissions and in Figure S 1 using ACCMIPv5, EDGAR_HTAPv2.2 and MACCity for the common stations. The comparison of surface simulated concentrations with observations showed NSD values above one, high nRMSE values and correlation coefficients below 0.5 in at most of the stations. The main difference from year 2013 is that the model-observation mismatches for the surface concentrations of the 12 BC species was estimated to be 32% in 2014 (Figure S 2), in contrast to 39% in 2013. The same deficiency of the model to capture the spring and summer concentrations of BC was observed. The calculated mismatches were very low in at most of the lower latitude stations and increased towards the remote Arctic ones (Figure S 2).

Finally, in 2015 the comparison of surface concentrations for each of the 12 different BC species using the four different datasets (ECLIPSEv5, ACCMIPv5, EDGAR_HTAPv2.2 and MACCity) with observations showed again the same pattern as in the previous years with most of the NSD values to be above unity, high nRMSE values and low Pearson coefficients (Figure 3 and Figure S 1). The model-observation mismatches of BC concentrations (Figure S 2) were estimated as high as 43% for the stations where full measurements existed for the

Nikolaos Evangeliou 27/9/2018 11:26
**Deleted:** Figure 3

Nikolaos Evangeliou 27/9/2018 11:26
**Deleted:** Figure S 1

Nikolaos Evangeliou 27/9/2018 11:26
**Deleted:** Figure S 2

Nikolaos Evangeliou 27/9/2018 11:26
**Deleted:** Figure S 2

Nikolaos Evangeliou 27/9/2018 11:26
**Deleted:** Table 2

Nikolaos Evangeliou 27/9/2018 11:26
**Deleted:** Figure 3

Nikolaos Evangeliou 27/9/2018 11:26
**Deleted:** Figure S 1

Nikolaos Evangeliou 27/9/2018 11:26
**Deleted:** Figure S 2

Nikolaos Evangeliou 27/9/2018 11:26
**Deleted:** Figure S 2

Nikolaos Evangeliou 27/9/2018 11:26
**Deleted:** Figure 3

Nikolaos Evangeliou 27/9/2018 11:26
**Deleted:** Figure S 1

Nikolaos Evangeliou 27/9/2018 11:26
**Deleted:** Figure S 2

three years of the study (2013–2015). Like in the previous years, the model failed to reproduce surface concentrations of BC at some of the remote stations of the Arctic.

We used the NMSE (Normalised Mean Square Error) to select the most representative BC tracer species. The NMSE is an estimator of the overall deviations between predicted and measured values. It is defined as:

$$NMSE = \frac{1}{N}\sum_i \frac{(O_i - P_i)^2}{\bar{P}_i \bar{O}_i} \qquad (5)$$

where $O_i$ and $P_i$ are observed and predicted concentrations, N the number of observations for which we assess the predicted values, while the overbar indicates the mean over the number of observations for $O_i$ and $P_i$. Contrary to the relative mismatches, in the NMSE the squared deviations (absolute values) are summed instead of the differences. For this reason, the NMSE generally shows the most striking differences among models. NMSE is a highly selective statistical quantity that can give large differences between models that perform similarly for other statistical measures. The lower the NMSE value, the better the performance of the model. On the other hand, high NMSE values do not necessarily mean that a model is completely wrong as the errors could be due to shifts in time and/or space. Moreover, it must be pointed out that NMSE is sensitive to outliers (Poli and Cirillo, 1993).

The calculated monthly average NMSE values for the 12 species using ECLIPSEv5 as the emission input can be seen in Figure 4 for year 2013–2015. The different scavenging coefficients used did not create a large variability in the monthly BC concentrations. This was caused due to the small perturbation of the scavenging coefficients. A more drastic change of wet scavenging would have caused BC concentrations to change more, as wet scavenging dominates removal and deposition of BC by approximately 80%. However, considering that the selection of the best representative species for BC was top priority, an effort to set realistic values to the scavenging coefficients was made. The best performance for the majority of the stations examined and most months was obtained for species 1, 2 and 10 (see Table 2). In terms of model response over the Arctic stations, a better performance was achieved for species 1 than for the other two. Therefore, we have chosen species 1 as our reference species for all subsequent analyses and the inversions. It should be noted here that the same test was performed using ACCMIPv5, EDGAR_HTAPv2.2 and MACCity emissions. Although the results were worse, the best-performed species for BC were again 1, 2 and 10.

Nikolaos Evangeliou 27/9/2018 11:26
**Deleted:** Figure 4

Nikolaos Evangeliou 21/9/2018 11:28
**Deleted:** variation

Nikolaos Evangeliou 21/9/2018 11:28
**Deleted:** of BC

Nikolaos Evangeliou 27/9/2018 11:26
**Deleted:** Table 2

### 3.2 Sensitivity to different prior information and selection of the best prior emission inventory

In this section we assess the impact of using the different prior emission inventories for BC and select the most appropriate one for our BC inversions. For this analysis, the best performing species 1 for BC (see Table 2) was chosen and the monthly relative model – observation mismatches ($([model - observations]/observations$) for all stations and years separated were calculated using all four inventories and are depicted in Figure S 3.

The largest monthly relative model-observation mismatches for the a priori simulated concentrations of BC in 2013 were calculated for stations located close to 50°N (BOS, CAB MEL, LEI, ULM, ANB). The average model-observation mismatch for all stations was 15% for 2013. Similar results were found for 2014 for the prior simulated BC concentrations with the largest relative mismatches recorded at mid-latitude stations where the BC concentrations were very high due to large anthropogenic emissions (BOS, CAB, MEL, LEI). On average, the relative model-observation mismatch was as high as 23% for the year 2014. Finally, in 2015, again the highest monthly relative mismatches of the a priori BC concentrations were estimated for the stations of high anthropogenic influence (CAB, MEL, LEI, WLD). The average relative model-observation mismatch in 2015 was only 19%, much lower than all previous years. The fact that all prior emission datasets used failed to reproduce the observations in central Europe during all years studied (2013, 2014 and 2015), whereas other stations at mid-latitudes were reproduced well, might imply either missing sources or highly uncertain measurements (Figure S 3). The use of different emission dataset changes simulated concentrations by a maximum of 23%.

Normalized mean square error (NMSE) values calculated for each of the four emission inventories were very low at the majority of the stations for which data existed in all the years of study (ZEP, SUM, TIK, BAR, MEL and LEI), when ECLIPSEv5 emissions were used. In contrast, at PAL all emission datasets performed well (Figure 5). The observations of BC concentrations at Arctic stations were better reproduced in simulations using the ECLIPSEv5 than with any other inventories examined. Law and Stohl (2007) have documented that these elevated BC concentrations are caused by anthropogenic emissions. Black carbon concentrations at TIK are not well simulated for reasons given in section 3.1.

### 3.3 Optimised (a posteriori) emissions of BC and associated uncertainty

The optimised annual emissions of BC together with the associated posterior gridded uncertainty and the difference between posterior and prior emissions averaged for the 2013–

Nikolaos Evangeliou 27/9/2018 11:26
**Deleted:** Table 2

Nikolaos Evangeliou 27/9/2018 11:26
**Deleted:** Figure S 3

Nikolaos Evangeliou 27/9/2018 11:26
**Deleted:** Figure S 3

Nikolaos Evangeliou 20/9/2018 15:49
**Deleted:** at maximum

Nikolaos Evangeliou 20/9/2018 15:51
**Deleted:** ,

Nikolaos Evangeliou 20/9/2018 15:51
**Deleted:** while

Nikolaos Evangeliou 27/9/2018 11:26
**Deleted:** Figure 5

Nikolaos Evangeliou 20/9/2018 15:52
**Deleted:** At most of the Arctic stations, the simulations using ECLIPSEv5 reproduced the observations better compared to the other inventories examined.

Nikolaos Evangeliou 20/9/2018 15:53
**Deleted:** (

Nikolaos Evangeliou 20/9/2018 15:53
**Deleted:** ,

Nikolaos Evangeliou 20/9/2018 15:53
**Deleted:** This shows that the most appropriate emission dataset for our purpose is the ECLIPSEv5 inventory, as it is the only one that can capture the characteristically elevated concentrations of BC in the Arctic, which persist until spring, and are caused by anthropogenic emissions (Law and Stohl, 2007).

Nikolaos Evangeliou 20/9/2018 15:54
**Deleted:** A significant deficiency is found for TIK for reasons that were explained earlier (see section

Nikolaos Evangeliou 20/9/2018 15:54
**Deleted:** )

2015 period can be seen in Figure 6. The posterior emissions are presented for the best performing species (species 1) of BC and the best prior emissions inventory (ECLIPSEv5). The total posterior uncertainty was calculated as the standard deviation of the posterior emissions calculated for the 12 BC species with different scavenging coefficients for four different emission datasets as prior information for each of the three years (12×4=48 inversions, see section 2.2). The total uncertainty is a propagation of the deposition uncertainty (represented by the posterior emissions using 12 perturbed BC species with different scavenging coefficients) and the uncertainty due to the use of different prior information (represented by the posterior emissions using the four different emission datasets). Table 3 reports annual prior, posterior, and averaged over 2013-2015, BC emissions for different regions. Five different regions are accounted for, namely North America, North Europe (including European Russia), North Siberia, Nenets-Komi (Russia) and Khanty-Mansiysk district (Russia).

The optimised emissions show some constant hot-spot areas that persist throughout all three years and which are attributed to anthropogenic BC emissions. For instance, emissions in the Nenets – Komi region close to the Yamal peninsula in Russia or in Khanty Mansiysk region of Northwestern Siberia have been reported to originate to a large extent from gas flaring (Popovicheva et al., 2017; Stohl et al., 2013; Winiger et al., 2017). Other areas that are characterised by large anthropogenic emissions are in Western Canada (Alberta), where more than 100 power industries burn fossil fuels and more than 50 oil and gas production and oil refining industries operate. In addition, one of the largest oil sands deposits are found in Northern Alberta and in the McMurray area, which contains about 168 billion barrels of oil (Heins, 2000). Cheng et al. (2018) found high concentrations of BC (more than 1000 ng $m^{-3}$) in the Canadian oil sands region at altitudes of up to 2 km during a flight campaign.

The optimised BC emissions in North America for the 2013–2015 period were between 149 and 193 kt $y^{-1}$ (average ± 1-sigma error: 174±58 kt $y^{-1}$), in the same order with the prior emissions in ECLIPSEv5 (148–182 kt $y^{-1}$) and slightly higher than ACCMIPv5, EDGAR_HTAPv2.2 and MACCity (116–150 kt $y^{-1}$). In Northern Europe we estimated that 124–238 kt $y^{-1}$ of BC were released (average ± 1-sigma error: 170±59 kt $y^{-1}$), which is less than half the ECLIPSEv5 emissions (352–381 kt $y^{-1}$), about 35% lower than the ACCMIPv5 and MACCity emissions (241 – 256 kt $y^{-1}$) and in the same order as the EDGAR_HTAPv2.2 emissions (163–175 kt $y^{-1}$). Posterior BC emissions were higher in North Siberia for the 3-year period (130–291 kt $y^{-1}$, average ± 1-sigma error: 217±69 kt $y^{-1}$) compared with ECLIPSEv5 (187–238 kt $y^{-1}$), ACCMIPv5 (127–178 kt $y^{-1}$), EDGAR_HTAPv2.2 (108–159 kt

Nikolaos Evangeliou 27/9/2018 11:26
**Deleted:** Figure 6

Nikolaos Evangeliou 26/9/2018 14:24
**Deleted:** were calculated

Nikolaos Evangeliou 27/9/2018 11:26
**Deleted:** 2.3

Nikolaos Evangeliou 25/9/2018 10:03
**Deleted:** combination

Nikolaos Evangeliou 27/9/2018 11:26
**Deleted:** Table 3

Nikolaos Evangeliou 20/9/2018 15:56
**Deleted:** and

Nikolaos Evangeliou 20/9/2018 15:56
**Deleted:**

Nikolaos Evangeliou 20/9/2018 15:56
**Deleted:** emissions of BC for different regions and average emissions for the period 2013–2015

Nikolaos Evangeliou 20/9/2018 15:58
**Deleted:** emissions of BC

Nikolaos Evangeliou 20/9/2018 16:03
**Deleted:** emissions of BC

Nikolaos Evangeliou 20/9/2018 16:03
**Deleted:** emissions of BC

$y^{-1}$) or MACCity (129–179 kt $y^{-1}$). Larger changes in the BC emissions were calculated in Russian territories that are known to be important gas flaring sources (Stohl et al., 2013). BC emissions in the Nenets-Komi oblast were between 14 and 17 kt $y^{-1}$ (average ± 1-sigma error: 15±5 kt $y^{-1}$), about 40% lower than the respective emissions in ECLIPSEv5 (≈25 kt $y^{-1}$), the only prior dataset that took gas flaring into account there. This could be due to the decreasing magnitude of the flaring emissions in the last few years (see Huang and Fu, 2016). Finally, in Khanty-Mansiysk BC emissions were 28–37 kt $y^{-1}$ (average ± 1-sigma error: 32±8 kt $y^{-1}$) compared to 25 kt $yr^{-1}$ in ECLIPSEv5, whereas in the other datasets that do not include BC emissions due to flaring, BC emissions were negligible. However, the posterior Khanty-Mansiysk emissions are shifted further east compared to the prior.

The annual posterior BC emissions at latitudes above 50°N were estimated as 560±171 kt $yr^{-1}$ averaged for the 2013–2015 time period (523±92 kt $yr^{-1}$ in 2013, 608±104 kt $yr^{-1}$ in 2014 and 549±100 kt $yr^{-1}$ in 2015, respectively). For the same area and period, BC emissions in ECLIPSEv5 were 745 kt $yr^{-1}$, in ACCMIPv5 533 kt $yr^{-1}$, in EDGAR_HTAPv2.2 437 kt $yr^{-1}$, while in MACCity they were 538 kt $yr^{-1}$. The annual posterior absolute uncertainty can be seen in Figure 6b. As it was explained before, this uncertainty is a combination of the uncertainty due to scavenging and due to the use of different prior information in the inversions of BC. Averaged over the period 2013-2015, the relative uncertainty of the inversion was estimated to be 30%. The uncertainty due to different scavenging coefficients in the BC species used was 25%, while the uncertainty due to the use of different prior emissions was only 5%.

### 3.4 Validation of the posterior emissions of BC

The concentrations of BC at eight measurement stations simulated with the posterior (optimised) BC emissions can be seen in Figure S 4. As expected, BC concentrations match the observations significantly better than using any of the a priori datasets with correlation coefficients above 0.6 for most of the stations. At the same time, NSD values were close to unity or lower and the nRMSE values below 1.5 at most of the stations shown in Figure S 4. However, the comparison to observations included in the inversion is not a sufficient indicator of the inversion's performance, as the inversion is designed to reduce the model-observation mismatches. The magnitude of the posterior reduction of the model mismatch to the observations is partly determined by the weighting given to the observations relative to the prior emissions. A much better performance indicator is the comparison of the posterior

Nikolaos Evangeliou 20/9/2018 15:59
**Deleted:** emissions of BC

Nikolaos Evangeliou 20/9/2018 15:59
**Deleted:** Emissions of BC

Nikolaos Evangeliou 20/9/2018 15:59
**Deleted:** emissions of BC

Nikolaos Evangeliou 20/9/2018 15:59
**Deleted:** emissions of BC

Nikolaos Evangeliou 20/9/2018 16:03
**Deleted:** emissions of BC

Nikolaos Evangeliou 27/9/2018 11:26
**Deleted:** Figure 6

Nikolaos Evangeliou 20/9/2018 16:10
**Deleted:** The relative uncertainty of the inversion averaged over the period 2013 to 2015 was estimated to be 30%.

Nikolaos Evangeliou 20/9/2018 16:03
**Deleted:** emissions of BC

Nikolaos Evangeliou 27/9/2018 11:26
**Deleted:** Figure S 4

Nikolaos Evangeliou 27/9/2018 11:26
**Deleted:** Figure S 4

concentrations with observations that were not included in the inversion (independent observations).

For this reason, we compared posterior BC concentrations with observations from the ACCACIA (Aerosol-Cloud Coupling and Climate Interactions in the Arctic) flight campaign, which was conducted near Zeppelin station, Ny-Ålesund, for 3 days in March 2013 (Sinha et al., 2017). This campaign was chosen because it was conducted during one year for which inversion results are available (2013). The results are shown in Figure 7, for the prior simulated concentrations of BC using four different emission datasets (ACCMIPv5, ECLIPSEv5, EDGAR_HTAPv2.2 and MACCity) and the posterior simulated BC concentrations. In all profiles, use of the optimised BC emissions results in a better agreement between modeled concentrations and observations compared to the prior simulated BC concentrations, while the RMSE (not normalised) values decrease substantially. However, the Pearson's correlation coefficients were below 0.5.

To assess the performance of the inversions of BC in 2014, we used an independent dataset from a ship campaign that took place in the North Atlantic and Baltic Seas in June and August 2014 (Figure 8) provided by Shevchenko et al. (2016). Although the measurements may sometimes be affected by the ship's exhaust, the posterior RMSE was 34% lower than the average RMSE using four different a priori emission datasets (ACCMIPv5, ECLIPSEv5, EDGAR_HTAPv2.2 and MACCity), supporting the view that the inversion improved the emissions for 2014.

To validate the 2015 inversions of BC, measurements from a ship campaign over the Russian Arctic were used (Popovicheva et al., 2017) and the results are shown in Figure 9. The cruise started from the port of Arkhangelsk in the Northwestern European Russia, reached the Bolshevik Island in the higher Russian Arctic and returned following more or less the same pathway. The calculated RMSE of the posterior BC concentrations with the measurements taken during the cruise was about 10% lower that the respective RMSE from the prior simulated concentrations of BC (average for all prior simulated emissions). This shows that the optimised emissions improved BC concentrations over the Russian Arctic. Some episodic peaks of BC throughout the ship cruise, however, were poorly captured.

## 4 Discussion

Nikolaos Evangeliou 27/9/2018 11:26
**Deleted:** Figure 7

Nikolaos Evangeliou 20/9/2018 16:03
**Deleted:** emissions of BC

Nikolaos Evangeliou 27/9/2018 11:26
**Deleted:** Figure 8

Nikolaos Evangeliou 27/9/2018 11:26
**Deleted:** Figure 9

## 4.1 BC emissions in North America

The spatial distribution of the optimised BC emissions in North America averaged for the 3-year period is depicted in Figure 10 and the annual posterior emissions for 2013, 2014 and 2015 are shown in Figure S 5. The right panel of the same figures shows the differences between posterior and prior emissions (ECLIPSEv5) and highlights the biggest emission changes compared to the a priori dataset.

The most characteristic locations of sources between 2013 and 2015 lie in Alberta, where most of the large oil-producing industries operate (Figure 10 and Figure S 5). The highest emission source was located in 60°N–135°W in 2013 and 2015, but not in 2014. This spot corresponds to the location of Whitehorse, which is the capital and only city of Yukon, and the largest city in Northern Canada. The area involves mining activities (mainly for gold) and three natural gas wells, while biomass in the form of cordwood and pellets is used for space heating (Yukon Government, 2018). The fact that near-zero BC emissions were calculated in Whitehorse in 2014 might be due to the lack of available measurements in North America, which in turn results in poorly constrained posterior BC emissions. Another similar hotspot area that is more intense in 2013 and 2015, but not in 2014 is located in Yellowknife north of Great Slave Lake (62.5°N–115°W, Figure S 5). The city is known for gold and diamond mining and an oil-driven power plant (Northwest Territories Power Corporation, https://www.ntpc.com). Finally, another characteristic hotspot emission region of BC is seen southeast of Lake Athabasca (57°N–108°W, Figure 10). Uranium mines are located in this region. These mines use diesel generators, diesel trucks, and other diesel-powered machinery. Exactly in this location, the Visible Infrared Imaging Radiometer Suite (VIIRS) showed relatively strong night-time light sources (https://www.lightpollutionmap.info/#zoom=5&lat=8255540&lon=-11864816&layers=B0FFFTFFFT).

## 4.2 BC emissions in Northern Europe

The posterior BC emissions in Northern Europe averaged for the period 2013–2015 can be seen in Figure 11, together with the difference between prior (ECLIPSEv5) and posterior BC emissions, while the posterior emissions for each individual year are shown in Figure S 6. The location of the gas flaring facilities are also presented in the same figures together with vegetation fires from the FEINE (Fire Emission Inventory– northern Eurasia) inventory (Hao et al., 2016). The latter combines the MODIS thermal anomalies products (MOD14 and MYD14) and the MODIS top-of-the-atmosphere-calibrated reflectance product (MOD02) to

Nikolaos Evangeliou 20/9/2018 16:03
**Deleted:** emissions of BC

Nikolaos Evangeliou 27/9/2018 11:26
**Deleted:** Figure 10

Nikolaos Evangeliou 27/9/2018 11:26
**Deleted:** Figure S 5

Nikolaos Evangeliou 20/9/2018 16:11
**Deleted:** In the same figures the differences between posterior and prior emissions (ECLIPSEv5) are shown (right panels) to indicate the biggest emission changes compared to the a priori dataset.

Nikolaos Evangeliou 27/9/2018 11:26
**Deleted:** Figure 10

Nikolaos Evangeliou 27/9/2018 11:26
**Deleted:** Figure S 5

Nikolaos Evangeliou 20/9/2018 16:13
**Deleted:** seen

Nikolaos Evangeliou 20/9/2018 16:00
**Deleted:** emissions of BC

Nikolaos Evangeliou 20/9/2018 16:03
**Deleted:** emissions of BC

Nikolaos Evangeliou 27/9/2018 11:26
**Deleted:** Figure S 5

Nikolaos Evangeliou 27/9/2018 11:26
**Deleted:** Figure 10

Nikolaos Evangeliou 20/9/2018 16:14
**Deleted:** In this region four uranium mines are located that use diesel generators, diesel trucks, and likely also other diesel-powered machinery.

Nikolaos Evangeliou 20/9/2018 16:04
**Deleted:** emissions of BC

Nikolaos Evangeliou 27/9/2018 11:26
**Deleted:** Figure 11

Nikolaos Evangeliou 27/9/2018 11:26
**Deleted:** Figure S 6

map and date burn scars that are screened for false detections. Land cover classification of burned areas are taken from the MODIS land cover change product (MOD12) (Friedl et al., 2010). This dataset is considered more realistic than GFED4 due to the emission factors used for BC (May et al., 2014) and the different approach of burned area calculation (see Hao et al., 2016).

The highest posterior BC emissions are calculated for the Moscow megacity at 55°N–37.5°E, Berlin 52°N–14°E, Warsaw 52°N–21°E, Kyiv 50°N–30°E, Saint Petersburg 60°N–30°E, while London is slightly misplaced to the west (Figure 11). The Scandinavian countries have the lowest emissions, although domestic heating there can also be important (Andersen and Jespersen, 2016). The difference between prior and posterior emissions show that vegetation fires have a large impact on the BC emissions especially in Eastern Europe. In particular in 2015, the inversion produces large emission increases exactly where a large number of fire hot spots were found (see Figure S 6).

### 4.3 BC emissions in North Siberia

Figure 12 illustrates the average posterior BC emissions in Western Siberia for the 2013–2015 period together with the difference between the prior (ECLIPSEv5) and the posterior BC emissions, while Figure S 7 shows the respective BC emissions for each year individually, together with the flaring facilities and the vegetation fires similarly to the previous section.

The prior BC emissions from flaring in Nenets-Komi oblast are confirmed by the inversion, although the emissions are shifted further east, while the flaring emissions in Khanty-Mansiysk are probably underestimated in ECLIPSEv5 (see also Table 3). Vegetation fires are shown to correlate well with BC emissions for 2013 (60°N –70°N) and 2014 (50°N–60°N) (Figure S 7), but not in 2015. Hotspots of high emissions were found in Dudinka (88°E–70°N), a town on the Yenisei River and the administrative center of Taymyrsky Dolgano-Nenetsky District of Krasnoyarsk Krai, Russia, due to the Norilsk Mining and Smelting Factory extracting coal and ores. Furthermore, increase posterior BC emissions were estimated across the line that connects some important Russian cities (Yekaterinsburg to Chelyabinsk, 60°E–55°N). These cities have been reported to contribute large amounts of BC mainly from transportation (see Evangeliou et al., 2018). Another hotspot exists at 108°E–58°N that corresponds to VIIRS night-time lights (https://www.lightpollutionmap.info/#zoom=5.696666666666656&lat=8239438&lon=12096227&layers=B0FFFTFFFT). These emissions are attributed to flaring as four facilities are

Nikolaos Evangeliou 20/9/2018 16:04
**Deleted:** emissions of BC

Nikolaos Evangeliou 27/9/2018 11:26
**Deleted:** Figure 11

Nikolaos Evangeliou 27/9/2018 11:26
**Deleted:** Figure S 6

Nikolaos Evangeliou 27/9/2018 11:26
**Deleted:** Figure 12

Nikolaos Evangeliou 20/9/2018 16:04
**Deleted:** emissions of BC

Nikolaos Evangeliou 20/9/2018 16:04
**Deleted:** emissions of BC

Nikolaos Evangeliou 27/9/2018 11:26
**Deleted:** Figure S 7

Nikolaos Evangeliou 20/9/2018 16:00
**Deleted:** emissions of BC

Nikolaos Evangeliou 20/9/2018 16:04
**Deleted:** emissions of BC

Nikolaos Evangeliou 27/9/2018 11:26
**Deleted:** Table 3

Nikolaos Evangeliou 27/9/2018 11:26
**Deleted:** Figure S 7

Nikolaos Evangeliou 20/9/2018 16:04
**Deleted:** emissions of BC

collocated there (see Figure 12). Finally, high BC emissions originate from the Nizhny Novgorod oblast (44°E–55°N). The oblast ranks seventh in Russia in industrial output. Processing industries predominate in the local economy. The leading sectors of more than 650 industries are engineering and metalworking, followed by chemical and petrochemical industries and forestry, woodworking, and paper industries and one facility that flare gas (GGFR, Figure 12).

In the western part of Siberia, there are numerous sources of average or low intensity. However, there no known anthropogenic sources there. At the lowest part of the inversion domain, in the borders of Russia with Mongolia, the posterior emissions showed a large increase (Figure 6). These emissions are prevalent along the Trans-Siberian Railway. Human activities in the villages along the railway have been highlighted to be the major cause of the fires there.

### 4.4 Seasonal variability of BC emissions

The monthly optimised BC emissions are shown in Figure 13 for the three years of study (2013–2015) for the entire area north of 50°N, and separately for areas north of 50°N in North America, North Europe, North Siberia, Nenets-Komi oblast (Russia) and Khanty-Mansiysk (Russia). The last two regions are known to have large emissions from gas flaring. In the same figure the prior emissions from ECLIPSEv5, EDGAR_HTAPv2.2, ACCMIPv5 and MACCity are plotted for comparison.

The total posterior BC emissions (>50°N) show large seasonal variation (Figure 13a). The maximum emissions were calculated for summer months (July in 2013 and June in 2014 and 2015). In these months large emissions from biomass burning have been reported both in GFED4 (see burned area in Giglio et al., 2013), as well as in the FEINE inventory for Northern Eurasia (Hao et al., 2016). Separating the inversion domain into continental regions reveals where biomass burning is important. For instance, in North America (Figure 13b), although GFED4 that is included in all the prior emission datasets, shows a large emission peak for BC in summer implying that fires are important, our optimised emissions show a significantly smaller variability. This was not the case for North Europe (Figure 13c) where the largest seasonal BC emissions were found in July for 2013 and in May for 2015, while in 2014 the largest peak appeared in April. This is not seen in the prior emission datasets, which show weak monthly variation. The largest seasonal variations were calculated for Northern Siberia (Figure 13d) and BC emissions there control the overall seasonal pattern for the total optimised BC emissions (>50°N). A large month-to-month variability was estimated in the

Nikolaos Evangeliou 27/9/2018 11:26
**Deleted:** Figure 12

Nikolaos Evangeliou 20/9/2018 16:00
**Deleted:** emissions of BC

Nikolaos Evangeliou 27/9/2018 11:26
**Deleted:** Figure 12

Nikolaos Evangeliou 27/9/2018 11:26
**Deleted:** Figure 6

Nikolaos Evangeliou 20/9/2018 16:04
**Deleted:** emissions of BC

Nikolaos Evangeliou 27/9/2018 11:26
**Deleted:** Figure 13

Nikolaos Evangeliou 20/9/2018 16:04
**Deleted:** emissions of BC

Nikolaos Evangeliou 27/9/2018 11:26
**Deleted:** Figure 13

Nikolaos Evangeliou 20/9/2018 16:14
**Deleted:** By separating the inversion domain into continental regions, it is easily seen where biomass burning is important.

Nikolaos Evangeliou 27/9/2018 11:26
**Deleted:** Figure 13

Nikolaos Evangeliou 27/9/2018 11:26
**Deleted:** Figure 13

Nikolaos Evangeliou 20/9/2018 16:00
**Deleted:** emissions of BC

Nikolaos Evangeliou 20/9/2018 16:15
**Deleted:** was already

Nikolaos Evangeliou 27/9/2018 11:26
**Deleted:** Figure 13

Nikolaos Evangeliou 20/9/2018 16:00
**Deleted:** emissions of BC

Nikolaos Evangeliou 20/9/2018 16:04
**Deleted:** emissions of BC

Nenets-Komi oblast (Figure 13e), but no clear seasonal pattern. Finally, the largest monthly BC emissions in Khanty-Mansiysk oblast of Russia (Figure 13f) were calculated in April for 2013, July for 2014 and June for 2015 showing that a large share in the BC emissions in this region originate from biomass burning since the region is located at mid-latitudes (60°N–65°N) and is vulnerable to open fires.

## 5 Conclusions

We have optimised BC emissions at high northern latitudes (>50°N) for the 2013–2015 period using a Bayesian inversion tool, an atmospheric transport model and network of continuous measurements of BC. We performed a sensitivity study to assess the best representative species for BC according to the efficiency of in-cloud and below-cloud scavenging, and the best representative emission inventory to be used as the prior information for our inversion.

The perturbation of scavenging coefficients for BC in the simulated concentrations creates a relative model–observation mismatch of 32%–43% for the three years of study, whereas the use of different emission inventories has a less significant effect in the simulated concentrations showing a relative model–observation mismatch of 15%–23%.

The posterior BC emissions show characteristic hot-spots throughout all three years in the Nenets – Komi region close to the Yamal peninsula in Russia or in Khanty Mansiysk region of Northwestern Siberia, where gas flaring facilities are located and in Western Canada (Alberta), where more than 150 power and oil/gas production industries operate. The annual posterior BC emissions at latitudes above 50°N were estimated as 560±171 kt $yr^{-1}$, significantly smaller than in ECLIPSEv5 (745 kt $yr^{-1}$), which was used and the prior information in the inversions of BC (best representative emission dataset).

The uncertainty of the inversions was assessed using a model ensemble represented by 12 different scavenging coefficients for BC and four different prior emission datasets (12×4=48) for each of the three years of our study. We calculate a relative uncertainty of the inversion of 30% for the three years of our study.

The posterior simulated concentrations of BC showed a better agreement with independent observations adopted from flight and ship campaigns over the Arctic presenting, in all cases, up to three times lower RMSE values.

In North America, the posterior emissions were found similar to the a priori ones driven by anthropogenic sources, while biomass burning appeared to be insignificant. This was confirmed by satellite products that showed weak existence of active fire hot-spots.



Nikolaos Evangeliou 27/9/2018 11:26
**Deleted:** Figure 13

Nikolaos Evangeliou 25/9/2018 12:37
**Deleted:** likely as a consequence of errors in the inversion

Nikolaos Evangeliou 20/9/2018 16:00
**Deleted:** emissions of BC

Nikolaos Evangeliou 27/9/2018 11:26
**Deleted:** Figure 13

Nikolaos Evangeliou 20/9/2018 16:00
**Deleted:** emissions of BC

Nikolaos Evangeliou 20/9/2018 16:04
**Deleted:** emissions of BC

Nikolaos Evangeliou 20/9/2018 16:16
**Deleted:** We performed a sensitivity study to assess the best representative species for BC in terms of scavenging and removal and the best representative emission inventory to be used as the prior information for our inversion.

Nikolaos Evangeliou 20/9/2018 16:04
**Deleted:** emissions of BC

Nikolaos Evangeliou 20/9/2018 16:04
**Deleted:** emissions of BC

In North Europe, posterior emissions were estimated to be half compared to the prior ones, with the highest releases to be in megacities and due to biomass burning in Eastern Europe.

Finally, in North Siberia the larger emissions were calculated along the transect between Yekaterinsburg and Chelyabinsk, while flaring in Nenets-Komi oblast is probably overestimated in the a priori emissions. Increased emissions in the borders between Russia and Mongolia are probably due to biomass burning in villages along the Trans-Siberian Railway.

*Data availability.* All data generated for the present publication are stored on NIRD (https://www.uio.no/english/services/it/research/storage/nird-sigma.html) (project NS9419K) and can be obtained from the corresponding author upon request.

*Competing financial interests.* The authors declare no competing financial interests.

*Acknowledgements*. We would like to acknowledge the project entitled "Emissions of Short-Lived Climate Forcers near and in the Arctic (SLICFONIA)", which was funded by the NORRUSS research program (Project ID: 233642) and the project entitled "The Role of Short-Lived Climate Forcers in the Global Climate" funded by the KLIMAFORSK program (Project ID: 235548) of the Research Council of Norway. Also the Research Council of Norway strategic institute initiatives (SIS) project "SOCA-Signals from the Arctic OCean in the Atmosphere" is acknowledged. We also acknowledge partial support by the AMAP secretariat, as this work shall contribute to the next AMAP assessment on short-lived climate forcers. Work was performed at the Nordic Centre of Excellence eSTICC (eScience Tools for Investigating Climate Change in northern high latitudes), supported by NordForsk grant 57001. We thank IIASA (especially Chris Heyes and Zig Klimont) for providing the ECLIPSEv5 emission dataset for BC. Computational and storage resources for the FLEXPART simulations were provided by NOTUR (NN9419K) and NIRD (NS9419K). All results can be accessed upon request to the corresponding author of this manuscript.

*Author contributions*. NE performed the simulations, analyses and wrote the paper, RLT helped in the adaptation of FLEXINVERT for BC and commented on the paper, SE helped in the implementation of the experiments and AS coordinated, commented and wrote parts of the paper.

## References


Ackerman, a. S.: Reduction of Tropical Cloudiness by Soot, Science (80-. )., 288(5468), 1042–1047, doi:10.1126/science.288.5468.1042, 2000.

AMAP: AMAP assessment 2015: Black carbon and ozone as Arctic climate forcers, Arctic Monitoring and Assessment Programme (AMAP), Oslo, Norway., 2015.

Andersen, S. and Jespersen, M. G.: A Protocol for Measuring Emissions of Black Carbon and Organic Carbon from Residential Wood Burning. [online] Available from: http://webcache.googleusercontent.com/search?q=cache:T48eUfM_V6YJ:www.ccacoalition.org/en/file/2570/download%3Ftoken%3DNkBK2GWw+&cd=3&hl=no&ct=clnk&gl=no&client=safari, 2016.

Asmi, E., Kondratyev, V., Brus, D., Laurila, T., Lihavainen, H., Backman, J., Vakkari, V., Aurela, M., Hatakka, J., Viisanen, Y., Uttal, T., Ivakhov, V. and Makshtas, A.: Aerosol size distribution seasonal characteristics measured in Tiksi, Russian Arctic, Atmos. Chem. Phys., 16(3), 1271–1287, doi:10.5194/acp-16-1271-2016, 2016.

Benkovitz, C. M., Schwartz, S. E., Jensen, M. P., Miller, M. A., Easter, R. C. and Bates, T. S.: Modeling atmospheric sulfur over the Northern Hemisphere during the Aerosol Characterization Experiment 2 experimental period, J. Geophys. Res. D Atmos., 109(22), 1–28, doi:10.1029/2004JD004939, 2004.

Bond, T. C. and Bergstrom, R. W.: Light Absorption by Carbonaceous Particles: An Investigative Review, Aerosol Sci. Technol., 40(1), 27–67, doi:10.1080/02786820500421521, 2006.

Bond, T. C., Streets, D. G., Yarber, K. F., Nelson, S. M., Woo, J. H. and Klimont, Z.: A technology-based global inventory of black and organic carbon emissions from combustion, J. Geophys. Res. D Atmos., 109(14), 1–43, doi:10.1029/2003JD003697, 2004.

Bond, T. C., Doherty, S. J., Fahey, D. W., Forster, P. M., Berntsen, T., Deangelo, B. J., Flanner, M. G., Ghan, S., Kärcher, B., Koch, D., Kinne, S., Kondo, Y., Quinn, P. K., Sarofim, M. C., Schultz, M. G., Schulz, M., Venkataraman, C., Zhang, H., Zhang, S., Bellouin, N., Guttikunda, S. K., Hopke, P. K., Jacobson, M. Z., Kaiser, J. W., Klimont, Z., Lohmann, U., Schwarz, J. P., Shindell, D., Storelvmo, T., Warren, S. G. and Zender, C. S.: Bounding the role of black carbon in the climate system: A scientific assessment, J. Geophys. Res. Atmos., 118(11), 5380–5552, doi:10.1002/jgrd.50171, 2013.

Browse, J., Carslaw, K. S., Arnold, S. R., Pringle, K. and Boucher, O.: The scavenging processes controlling the seasonal cycle in Arctic sulphate and black carbon aerosol, Atmos.

Chem. Phys., 12(15), 6775–6798, doi:10.5194/acp-12-6775-2012, 2012.
Brunner, D., Arnold, T., Henne, S., Manning, A., Thompson, R. L., Maione, M., Doherty, S. O. and Reimann, S.: Comparison of four inverse modelling systems applied to the estimation of HFC-125 , HFC-134a , and SF 6 emissions over Europe, , 10651–10674, 2017.
Cao, G., Zhang, X. and Zheng, F.: Inventory of black carbon and organic carbon emissions from China, Atmos. Environ., 40(34), 6516–6527, doi:10.1016/j.atmosenv.2006.05.070, 2006.
Cheng, Y., Li, S., Gordon, M. and Liu, P.: Size distribution and coating thickness of black carbon from the Canadian oil sands operations, , 2004, 2653–2667, 2018.
Clarke, A. D. and Noone, K. J.: Soot in the arctic snowpack: a cause for perturbations in radiative transfer, Atmos. Environ., 41(SUPPL.), 64–72, doi:10.1016/0004-6981(85)90113-1, 1985.
Eckhardt, S., Quennehen, B., Olivié, D. J. L., Berntsen, T. K., Cherian, R., Christensen, J. H., Collins, W., Crepinsek, S., Daskalakis, N., Flanner, M., Herber, A., Heyes, C., Hodnebrog, Huang, L., Kanakidou, M., Klimont, Z., Langner, J., Law, K. S., Lund, M. T., Mahmood, R., Massling, A., Myriokefalitakis, S., Nielsen, I. E., Nøjgaard, J. K., Quaas, J., Quinn, P. K., Raut, J. C., Rumbold, S. T., Schulz, M., Sharma, S., Skeie, R. B., Skov, H., Uttal, T., Von Salzen, K. and Stohl, A.: Current model capabilities for simulating black carbon and sulfate concentrations in the Arctic atmosphere: A multi-model evaluation using a comprehensive measurement data set, Atmos. Chem. Phys., 15(16), 9413–9433, doi:10.5194/acp-15-9413-2015, 2015.
Elvidge, C. D., Ziskin, D., Baugh, K. E., Tuttle, B. T., Ghosh, T., Pack, D. W., Erwin, E. H. and Zhizhin, M.: A fifteen year record of global natural gas flaring derived from satellite data, Energies, 2(3), 595–622, doi:10.3390/en20300595, 2009.
Evangeliou, N., Balkanski, Y., Hao, W. M., Petkov, A., Silverstein, R. P., Corley, R., Nordgren, B. L., Urbanski, S. P., Eckhardt, S., Stohl, A., Tunved, P., Crepinsek, S., Jefferson, A., Sharma, S., Nøjgaard, J. K. and Skov, H.: Wildfires in northern Eurasia affect the budget of black carbon in the Arctic-a 12-year retrospective synopsis (2002-2013), Atmos. Chem. Phys., 16(12), 7587–7604, doi:10.5194/acp-16-7587-2016, 2016.
Evangeliou, N., Shevchenko, V. P., Yttri, K. E., Sollum, E., Pokrovsky, O. S., Kobelev, V. O., Vladimir, B., Lobanov, A. A., Starodymova, D. P., Vorobiev, S. N., Thompson, R. L., Stohl, A., Toulouse, G. E. and Belin, E.: Origin of elemental carbon in snow from Western Siberia and northwestern European Russia during winter – spring, Atmos. Chem. Phys., 18, 963–977, doi:10.5194/acp-18-963-2018, 2018.

869 Friedl, M. A., Sulla-Menashe, D., Tan, B., Schneider, A., Ramankutty, N., Sibley, A. and
870 Huang, X.: MODIS Collection 5 global land cover: Algorithm refinements and
871 characterization of new datasets, Remote Sens. Environ., 114(1), 168–182,
872 doi:10.1016/j.rse.2009.08.016, 2010.
873 Gelencsér, A., Hoffer, A., Molnár, A., Krivácsy, Z., Kiss, G. and Mészáros, E.: Thermal
874 behaviour of carbonaceous aerosol from a continental background site, Atmos. Environ.,
875 34(5), 823–831, doi:10.1016/S1352-2310(99)00206-X, 2000.
876 Giglio, L., Randerson, J. T. and van der Werf, G. R.: Analysis of daily, monthly, and annual
877 burned area using the fourth-generation global fire emissions database (GFED4), J. Geophys.
878 Res. Biogeosciences, 118, 317–328, doi:10.1002/jgrg.20042, 2013, 2013.
879 Government, Y.: Economic sectors, 2018.
880 Grythe, H., Kristiansen, N. I., Groot Zwaaftink, C. D., Eckhardt, S., Ström, J., Tunved, P.,
881 Krejci, R. and Stohl, A.: A new aerosol wet removal scheme for the Lagrangian particle
882 model FLEXPARTv10, Geosci. Model Dev., 10, 1447–1466, doi:10.5194/gmd-10-1447-
883 2017, 2017.
884 Hao, W. M., Petkov, A., Nordgren, B. L., Silverstein, R. P., Corley, R. E., Urbanski, S. P.,
885 Evangeliou, N., Balkanski, Y. and Kinder, B.: Daily black carbon emissions from fires in
886 Northern Eurasia from 2002 to 2013, Geosci. Model Dev., 9, 4461–4474, doi:10.5194/gmd-9-
887 4461-2016, 2016.
888 Hegg, D. A., Warren, S. G., Grenfell, T. C., Doherty, S. J., Larson, T. V. and Clarke, A. D.:
889 Source attribution of black carbon in arctic snow, Environ. Sci. Technol., 43(11), 4016–4021,
890 doi:10.1021/es803623f, 2009.
891 Heins, F. J.: Historical overview of the Fort McMurray area and oil sands industry in
892 Northeast Alberta. [online] Available from:
893 https://web.archive.org/web/20080227201038/http://www.ags.gov.ab.ca/publications/ESR/P
894 DF/ESR_2000_05.pdf, 2000.
895 Hodnebrog, Ø., Myhre, G. and Samset, B. H.: How shorter black carbon lifetime alters its
896 climate effect., Nat. Commun., 5(May), 5065, doi:10.1038/ncomms6065, 2014.
897 Huang, K. and Fu, J. S.: A global gas flaring black carbon emission rate dataset from 1994 to
898 2012, Nature, 3, 160104, doi:10.1038/sdata.2016.104, 2016.
899 Huang, K., Fu, J. S., Prikhodko, V. Y., Storey, J. M., Romanov, A., Hodson, E. L., Cresko, J.,
900 Morozova, I., Ignatieva, Y. and Cabaniss, J.: Russian anthropogenic black carbon: Emission
901 reconstruction and Arctic black carbon simulation, J. Geophys. Res. Atmos., 120(21), 11306–
902 11333, doi:10.1002/2015JD023358, 2015.

903 Janssens-Maenhout, G., Crippa, M., Guizzardi, D., Dentener, F., Muntean, M., Pouliot, G.,
904 Keating, T., Zhang, Q., Kurokawa, J., Wankmüller, R., Denier Van Der Gon, H., Kuenen, J. J.
905 P., Klimont, Z., Frost, G., Darras, S., Koffi, B. and Li, M.: HTAP-v2.2: A mosaic of regional
906 and global emission grid maps for 2008 and 2010 to study hemispheric transport of air
907 pollution, Atmos. Chem. Phys., 15(19), 11411–11432, doi:10.5194/acp-15-11411-2015, 2015.
908 Jinhuan, Q. and Liquan, Y.: Variation characteristics of atmospheric aerosol optical depths
909 and visibility in North China during 1980 } 1994, Atmos. Environ., 34, 603–609, 2000.
910 Klimont, Z., Kupiainen, K., Heyes, C., Purohit, P., Cofala, J., Rafaj, P., Borken-Kleefeld, J.
911 and Schöpp, W.: Global anthropogenic emissions of particulate matter including black
912 carbon, Atmos. Chem. Phys., 17, 8681–8723, doi:10.5194/acp-17- 50 8681-2017, 2017.
913 Klonecki, A.: Seasonal changes in the transport of pollutants into the Arctic troposphere-
914 model study, J. Geophys. Res., 108(D4), 8367, doi:10.1029/2002JD002199, 2003.
915 Koch, D. and Hansen, J.: Distant origins of Arctic black carbon: A Goddard Institute for
916 Space Studies ModelE experiment, J. Geophys. Res. D Atmos., 110(4), 1–14,
917 doi:10.1029/2004JD005296, 2005.
918 Lamarque, J. F., Bond, T. C., Eyring, V., Granier, C., Heil, A., Klimont, Z., Lee, D., Liousse,
919 C., Mieville, A., Owen, B., Schultz, M. G., Shindell, D., Smith, S. J., Stehfest, E., Van
920 Aardenne, J., Cooper, O. R., Kainuma, M., Mahowald, N., McConnell, J. R., Naik, V., Riahi,
921 K. and Van Vuuren, D. P.: Historical (1850-2000) gridded anthropogenic and biomass
922 burning emissions of reactive gases and aerosols: Methodology and application, Atmos.
923 Chem. Phys., 10(15), 7017–7039, doi:10.5194/acp-10-7017-2010, 2010.
924 Lamarque, J. F., Shindell, D. T., Josse, B., Young, P. J., Cionni, I., Eyring, V., Bergmann, D.,
925 Cameron-Smith, P., Collins, W. J., Doherty, R., Dalsoren, S., Faluvegi, G., Folberth, G.,
926 Ghan, S. J., Horowitz, L. W., Lee, Y. H., MacKenzie, I. A., Nagashima, T., Naik, V.,
927 Plummer, D., Righi, M., Rumbold, S. T., Schulz, M., Skeie, R. B., Stevenson, D. S., Strode,
928 S., Sudo, K., Szopa, S., Voulgarakis, A. and Zeng, G.: The atmospheric chemistry and climate
929 model intercomparison Project (ACCMIP): Overview and description of models, simulations
930 and climate diagnostics, Geosci. Model Dev., 6(1), 179–206, doi:10.5194/gmd-6-179-2013,
931 2013.
932 Law, K. S. and Stohl, A.: Arctic Air Pollution: Origins and Impacts, Science (80-. ).,
933 315(5818), 1537–1540, doi:10.1126/science.1137695, 2007.
934 Long, C. M., Nascarella, M. A. and Valberg, P. A.: Carbon black vs. black carbon and other
935 airborne materials containing elemental carbon: Physical and chemical distinctions, Environ.
936 Pollut., 181, 271–286, doi:10.1016/j.envpol.2013.06.009, 2013.

May, A. A., McMeeking, G. R., Lee, T., Taylor, J. W., Craven, J. S., Burling, I., Sullivan1, A. P., Akagi, S., Jr., J. L. C., Flynn, M., Coe, H., Urbanski, S. P., Seinfeld6, J. H., Yokelson8, R. J. and Kreidenweis, S. M.: Aerosol emissions from prescribed fires in the United States: A synthesis of laboratory and aircraft measurements, J. Geophys. Res. Atmos., 119, 11826–11849, doi:10.1002/ 2014JD021848, 2014.

Muller, T., Henzing, J. S., De Leeuw, G., Wiedensohler, A., Alastuey, A., Angelov, H., Bizjak, M., Collaud Coen, M., Engstr??m, J. E., Gruening, C., Hillamo, R., Hoffer, A., Imre, K., Ivanow, P., Jennings, G., Sun, J. Y., Kalivitis, N., Karlsson, H., Komppula, M., Laj, P., Li, S. M., Lunder, C., Marinoni, A., Martins Dos Santos, S., Moerman, M., Nowak, A., Ogren, J. A., Petzold, A., Pichon, J. M., Rodriquez, S., Sharma, S., Sheridan, P. J., Teinil??, K., Tuch, T., Viana, M., Virkkula, A., Weingartner, E., Wilhelm, R. and Wang, Y. Q.: Characterization and intercomparison of aerosol absorption photometers: Result of two intercomparison workshops, Atmos. Meas. Tech., 4(2), 245–268, doi:10.5194/amt-4-245-2011, 2011.

Myhre, G., Samset, B. H., Schulz, M., Balkanski, Y., Bauer, S., Berntsen, T. K., Bian, H., Bellouin, N., Chin, M., Diehl, T., Easter, R. C., Feichter, J., Ghan, S. J., Hauglustaine, D., Iversen, T., Kinne, S., Kirkeväg, A., Lamarque, J. F., Lin, G., Liu, X., Lund, M. T., Luo, G., Ma, X., Van Noije, T., Penner, J. E., Rasch, P. J., Ruiz, A., Seland, Skeie, R. B., Stier, P., Takemura, T., Tsigaridis, K., Wang, P., Wang, Z., Xu, L., Yu, H., Yu, F., Yoon, J. H., Zhang, K., Zhang, H. and Zhou, C.: Radiative forcing of the direct aerosol effect from AeroCom Phase II simulations, Atmos. Chem. Phys., 13(4), 1853–1877, doi:10.5194/acp-13-1853-2013, 2013.

Nordmann, S., Birmili, W., Weinhold, K., Müller, K., Spindler, G. and Wiedensohler, A.: Measurements of the mass absorption cross section of atmospheric soot particles using Raman spectroscopy, J. Geophys. Res. Atmos., 118(21), 12075–12085, doi:10.1002/2013JD020021, 2013.

Park, R. J., Jacob, D. J., Palmer, P. I., Clarke, A. D., Weber, R. J., Zondlo, M. A., Eisele, F. L., Bandy, A. R., Thornton, D. C., Sachse, G. W. and Bond, T. C.: Export efficiency of black carbon aerosol in continental outflow: Global implications, J. Geophys. Res. D Atmos., 110(11), 1–7, doi:10.1029/2004JD005432, 2005.

Petzold, A. and Schönlinner, M.: Multi-angle absorption photometry - A new method for the measurement of aerosol light absorption and atmospheric black carbon, J. Aerosol Sci., 35(4), 421–441, doi:10.1016/j.jaerosci.2003.09.005, 2004.

Petzold, A., Ogren, J. A., Fiebig, M., Laj, P., Li, S. M., Baltensperger, U., Holzer-Popp, T., Kinne, S., Pappalardo, G., Sugimoto, N., Wehrli, C., Wiedensohler, A. and Zhang, X. Y.:

971 Recommendations for reporting black carbon measurements, Atmos. Chem. Phys., 13(16),
972 8365–8379, doi:10.5194/acp-13-8365-2013, 2013.
973 Poli, A. A. and Cirillo, M. C.: On the use of the normalized mean square error in evaluating
974 dispersion model performance, Atmos. Environ. Part A, Gen. Top., 27(15), 2427–2434,
975 doi:10.1016/0960-1686(93)90410-Z, 1993.
976 Popovicheva, O. B., Evangeliou, N., Eleftheriadis, K., Kalogridis, A. C., Movchan, V.,
977 Sitnikov, N., Eckhardt, S., Makshtas, A. and Stohl, A.: Black carbon sources constrained by
978 observations and modeling in the Russian high Arctic, Environ. Sci. Technol., 51,
979 3871−3879, doi:10.1021/acs.est.6b05832, 2017.
980 Samset, B. H., Myhre, G., Herber, A., Kondo, Y., Li, S. M., Moteki, N., Koike, M., Oshima,
981 N., Schwarz, J. P., Balkanski, Y., Bauer, S. E., Bellouin, N., Berntsen, T. K., Bian, H., Chin,
982 M., Diehl, T., Easter, R. C., Ghan, S. J., Iversen, T., Kirkev??g, A., Lamarque, J. F., Lin, G.,
983 Liu, X., Penner, J. E., Schulz, M., Seland, Skeie, R. B., Stier, P., Takemura, T., Tsigaridis, K.
984 and Zhang, K.: Modelled black carbon radiative forcing and atmospheric lifetime in AeroCom
985 Phase II constrained by aircraft observations, Atmos. Chem. Phys., 14(22), 12465–12477,
986 doi:10.5194/acp-14-12465-2014, 2014.
987 Schaap, M., Denier Van Der Gon, H. A. C., Dentener, F. J., Visschedijk, A. J. H., Van Loon,
988 M., ten Brink, H. M., Putaud, J. P., Guillaume, B., Liousse, C. and Builtjes, P. J. H.:
989 Anthropogenic black carbon and fine aerosol distribution over Europe, J. Geophys. Res.
990 Atmos., 109(18), doi:10.1029/2003JD004330, 2004.
991 Schladitz, A., Leníček, J., Beneš, I., Kováč, M., Skorkovský, J., Soukup, A., Jandlová, J.,
992 Poulain, L., Plachá, H., Löschau, G. and Wiedensohler, A.: Air quality in the German-Czech
993 border region: A focus on harmful fractions of PM and ultrafine particles, Atmos. Environ.,
994 122, 236–249, doi:10.1016/j.atmosenv.2015.09.044, 2015.
995 Seibert, P. and Frank, A.: Source-receptor matrix calculation with a Lagrangian particle
996 dispersion model in backward mode, Atmos. Chem. Phys., 4(1), 51–63, doi:10.5194/acp-4-
997 51-2004, 2004.
998 Shevchenko, V. P., Kopeikin, V. M., Evangeliou, N., Lisitzin, A. P., Novigatsky, A. N.,
999 Pankratova, N. V, Starodymova, D. P., Stohl, A. and Thompson, R.: Atmospheric Black
1000 Carbon over the North Atlantic and the Russian Arctic Seas in Summer-Autumn Time,
1001 Химия В Интересах Устойчивого Развития, 24(4), 441–446,
1002 doi:10.15372/KhUR20160402, 2016.
1003 Sinha, P. R., Kondo, Y., Koike, M., Ogren, J. A., Jefferson, A., Barrett, T. E., Sheesley, R. J.,
1004 Ohata, S., Moteki, N., Coe, H., Liu, D., Irwin, M., Tunved, P., Quinn, P. K. and Zhao, Y.:

Evaluation of ground-based black carbon measurements by filter-based photometers at two Arctic sites, J. Geophys. Res., 122(6), 3544–3572, doi:10.1002/2016JD025843, 2017.

Slinn, W. G. N.: Predictions for particle deposition to vegetative canopies, Atmos. Environ., 16, 1785–1794, doi:10.1016/0004-6981(82)90271-2, 1982.

Stohl, A.: Characteristics of atmospheric transport into the Arctic troposphere, J. Geophys. Res. Atmos., 111(11), 1–17, doi:10.1029/2005JD006888, 2006.

Stohl, A., Hittenberger, M. and Wotawa, G.: Validation of the lagrangian particle dispersion model FLEXPART against large-scale tracer experiment data, Atmos. Environ., 32(24), 4245–4264, doi:10.1016/S1352-2310(98)00184-8, 1998.

Stohl, A., Forster, C., Frank, A., Seibert, P. and Wotawa, G.: Technical note: The Lagrangian particle dispersion model FLEXPART version 6.2, Atmos. Chem. Phys., 5(9), 2461–2474, doi:10.5194/acp-5-2461-2005, 2005.

Stohl, A., Seibert, P., Arduini, J., Eckhardt, S., Fraser, P., Greally, B. R., Maione, M., O'Doherty, S., Prinn, R. G., Reimann, S., Saito, T., Schmidbauer, N., Simmonds, P. G., Vollmer, M. K., Weiss, R. F. and Yokouchi, Y.: A new analytical inversion method for determining regional and global emissions of greenhouse gases: sensitivity studies and application to halocarbons, Atmos. Chem. Phys., 9, 1597–1620, doi:10.5194/acp-9-1597-2009, 2009.

Stohl, A., Klimont, Z., Eckhardt, S., Kupiainen, K., Shevchenko, V. P., Kopeikin, V. M. and Novigatsky, A. N.: Black carbon in the Arctic: The underestimated role of gas flaring and residential combustion emissions, Atmos. Chem. Phys., 13(17), 8833–8855, doi:10.5194/acp-13-8833-2013, 2013.

Streets, D. G., Bond, T. C., Carmichael, G. R., Fernandes, S. D., Fu, Q., He, D., Klimont, Z., Nelson, S. M., Tsai, N. Y., Wang, M. Q., Woo, J.-H. and Yarber, K. F.: An inventory of gaseous and primary aerosol emissions in Asia in the year 2000, J. Geophys. Res., 108(D21), 8809, doi:10.1029/2002JD003093, 2003.

Tarantola, A.: Inverse Problem Theory and Methods for Model Parameter Estimation, Society for Industrial and Applied Mathematics, Philadelphia, Pa., 2005.

Textor, C., Schulz, M., Guibert, S., Kinne, S., Balkanski, Y., Bauer, S., Berntsen, T., Berglen, T., Boucher, O., Chin, M., Dentener, F., Diehl, T., Easter, R., Feichter, H., Fillmore, D., Ghan, S., Ginoux, P., Gong, S., Grini, a., Hendricks, J., Horowitz, L., Huang, P., Isaksen, I., Iversen, T., Kloster, S., Koch, D., Kirkevåg, a., Kristjansson, J. E., Krol, M., Lauer, a., Lamarque, J. F., Liu, X., Montanaro, V., Myhre, G., Penner, J., Pitari, G., Lamarque, J. F., Liu, X., Montanaro, V., Myhre, G., Penner, J., Pitari, G., Reddy, S., Seland, Ø., Stier, P.,

Takemura, T. and Tie, X.: Analysis and quantification of the diversities of aerosol life cycles within AeroCom, Atmos. Chem. Phys., 6, 1777–1813, doi:10.5194/acpd-5-8331-2005, 2006.

Thacker, W. C.: Data assimilation with inequality constraints, Ocean Model., 16(3–4), 264–276, doi:10.1016/j.ocemod.2006.11.001, 2007.

Thompson, R. L. and Stohl, A.: FLEXINVERT: An atmospheric Bayesian inversion framework for determining surface fluxes of trace species using an optimized grid, Geosci. Model Dev., 7(5), 2223–2242, doi:10.5194/gmd-7-2223-2014, 2014.

Thompson, R. L., Stohl, A., Zhou, L. X., Dlugokencky, E., Fukuyama, Y., Tohjima, Y., Kim, S. Y., Lee, H., Nisbet, E. G., Fisher, R. E., Lowry, D., Weiss, R. F., Prinn, R. G., O'Doherty, S., Young, D. and White, J. W. C.: Methane emissions in East Asia for 2000-2011 estimated using an atmospheric Bayesian inversion, J. Geophys. Res. Atmos., 120(9), 4352–4369, doi:10.1002/2014JD022394, 2015.

Thompson, R. L., Sasakawa, M., Machida, T., Aalto, T., Worthy, D., Lavric, J. V., Lund Myhre, C. and Stohl, A.: Methane fluxes in the high northern latitudes for 2005-2013 estimated using a Bayesian atmospheric inversion, Atmos. Chem. Phys., 17, 3553–3572, doi:10.5194/acp-17-3553-2017, 2017.

Wang, P., Wang, H., Wang, Y. Q., Zhang, X. Y., Gong, S. L., Xue, M., Zhou, C. H., Liu, H. L., An, X. Q., Niu, T. and Cheng, Y. L.: Inverse modeling of black carbon emissions over China using ensemble data assimilation, Atmos. Chem. Phys., 16(2), 989–1002, doi:10.5194/acp-16-989-2016, 2016.

Wang, R., Tao, S., Balkanski, Y., Ciais, P., Boucher, O., Liu, J., Piao, S., Shen, H., Vuolo, M. R., Valari, M., Chen, H., Chen, Y., Cozic, A., Huang, Y., Li, B., Li, W., Shen, G., Wang, B. and Zhang, Y.: Exposure to ambient black carbon derived from a unique inventory and high-resolution model., Proc. Natl. Acad. Sci. U. S. A., 111(7), 2459–63, doi:10.1073/pnas.1318763111, 2014.

Winiger, P., Andersson, A., Eckhardt, S., Stohl, A., Semiletov, I. P., Dudarev, O. V., Charkin, A., Shakhova, N., Klimont, Z., Heyes, C. and Gustafsson, Ö.: Siberian Arctic black carbon sources constrained by model and observation, Proc. Natl. Acad. Sci., 114(7), E1054–E1061, doi:10.1073/pnas.1613401114, 2017.

## TABLES & LEGENDS

**Table 1.** Observation sites used for the inversions (the altitude indicates the sampling height in meters above sea level).

| Site ID | Organisation | Latitude | Longitude | Altitude | Year | Instrument | Description |
|---|---|---|---|---|---|---|---|
| ALT | EC/AES | 82.5°N | 62.5°W | 205 m | 2013, 2015 | PSAP-3W | Alert, Nunavut, Canada |
| ANB | HMGU | 50.6°N | 13.0°E | 549 m | 2013 | MAAP | Annaberg-Buchholz, Germany |
| APP | AAIRF | 36.2°N | 81.7°W | 1110 m | 2015 | PSAP-3W | Appalachian SU, Boone, USA |
| ASP | SU | 58.8°N | 17.4°E | 20 m | 2013 | PSAP | Asprveten, Västerås, Sweden |
| BAR | NOAA-ESRL | 71.3°N | 161.6°W | 9 m | 2013, 2014, 2015 | CLAP-3W | Barrow, Alaska, USA |
| BIR | NILU | 58.4°N | 8.2°E | 219 m | 2014, 2015 | PSAP-3W | Birkenes, Norway |
| BON | NOAA-ESRL | 40.0°N | 88.4°W | 213 | 2015 | CLAP-3W | Bondville, USA |
| BOS | TROPOS | 53.0°N | 7.9°E | 53 m | 2013, 2014 | MAAP-5012 | Bösel, Germany |
| CAB | ACTRIS, GAW | 52.0°N | 4.9°E | 61 m | 2013, 2014, 2015 | Thermo-5012 | Cabauw Zijdeweg, Netherlands |
| COL | NOAA-ESRL | 40.4°N | 106.7°W | 3220 m | 2015 | PSAP-3W | Steamboat Springs, Colorado, USA |
| ETL | EC/AES | 54.4°N | 105.0°W | 502 m | 2013, 2015 | PSAP-1W | East Trout Lake, Canada |
| GOS | NOAA | 33.3°N | 126.2°E | 72 m | 2014, 2015 | CLAP-3W | Gosan, South Korea |
| HYY | UH, DPS | 61.6°N | 24.2°E | 181 m | 2013, 2015 | Thermo-5012 | Hyytiälä, Finland |
| KPU | HMS, ACUV | 47.0°N | 19.6°E | 125 m | 2013, 2014, 2015 | CLAP-3W | K-puszta, Hungary |
| LEI | TROPOS | 51.3°N | 12.3°E | 122 m | 2013, 2014, 2015 | MAAP-5012 | Leipzig, Germany |
| MEL | TROPOS | 51.5°N | 12.9°E | 86 m | 2013, 2014, 2015 | MAAP-5012 | Melpitz, Torgau, Germany |
| MOU | ACTRIS, GAW | 42.2°N | 23.6°E | 2971 m | 2014, 2015 | CLAP-3W | BEO Moussala, Bulgaria |
| MOV | - | 38.1°N | 8.8°W | 43 m | 2015 | RFPS-1287 | Monte Velho, Portugal |
| NEP | CNR | 28.0°N | 86.8°E | 5079 m | 2015 | MAAP01 | Nepal Climate Observatory |
| PAL | FMI | 68.0°N | 24.2°E | 560 m | 2013, 2014, 2015 | Thermo-5012 | Pallas, Sodankylä, Finland |
| SGP | NOAA-ESRL | 36.6°N | 97.5°W | 318 m | 2015 | PSAP-3W | South Great Planes, USA |
| SUM | PF | 72.6°N | 38.5°W | 3211 m | 2013, 2014, 2015 | CLAP-3W | Summit, Greenland |
| TIK | NOAA, MeteoRF | 71.6°N | 128.9°E | 30 m | 2013, 2014, 2015 | Magee AE31 | Tiksi, Russian Federation |
| TRI | NOAA-ESRL | 41.1°N | 124.2°W | 117 m | 2015 | PSAP-3W | Trinidad Head, Canada |
| ULM | ACTRIS, GAW | 50.7°N | 14.8°E | 161 m | 2013 | MAAP-CHMI | Ústí n.L.-mesto, Czechia |
| WHI | EC/AES | 50.0°N | 122.9°W | 2182 m | 2013, 2015 | PSAP-1W | Whisper, British Columbia, Canada |
| WLD | GAW-WDCA | 52.8°N | 10.8°E | 78 m | 2015 | MAAP-5012 | Waldhof, Germany |
| ZEP | NCSRD | 78.9°N | 11.9°E | 474 m | 2013, 2014, 2015 | Magee AE31 | Zeppelin, Ny Ålesund, Norway |

**Table 2.** Different scavenging parameters of below–cloud and in–cloud scavenging used in the ensemble model simulations for BC. $A_{\downarrow}$ and $B_{\downarrow}$ are rain and snow collection efficiencies for below-cloud scavenging, $A_{i\downarrow}$ is the cloud condensation nuclei efficiency and $B_{i\downarrow}$ the ice nuclei efficiency that are used in in-cloud scavenging following Grythe et al. (2017).

| | $A_{\downarrow}$ | $B_{\downarrow}$ | $A_{i\downarrow}$ | $B_{i\downarrow}$ |
|---|---|---|---|---|
| BC1 | 1.0 | 1.0 | 0.90 | 0.10 |
| BC2 | 1.0 | 1.0 | 0.90 | 0.45 |
| BC3 | 1.0 | 1.0 | 0.45 | 0.20 |
| BC4 | 1.0 | 0.5 | 0.45 | 0.20 |
| BC5 | 0.5 | 0.5 | 0.45 | 0.20 |
| BC6 | 1.0 | 0.2 | 0.90 | 0.20 |
| BC7 | 1.0 | 1.0 | 0.20 | 0.20 |
| BC8 | 2.0 | 1.0 | 0.45 | 0.10 |
| BC9 | 0.2 | 0.2 | 0.90 | 0.90 |
| BC10 | 1.0 | 1.0 | 0.90 | 0.20 |
| BC11 | 2.0 | 1.0 | 0.45 | 0.45 |
| BC12 | 1.0 | 1.0 | 0.45 | 0.00 |

Nikolaos Evangeliou 25/9/2018 12:52
**Deleted:** A

Nikolaos Evangeliou 25/9/2018 12:52
**Deleted:** B

Nikolaos Evangeliou 25/9/2018 12:53
**Deleted:** Ai

Nikolaos Evangeliou 25/9/2018 12:53
**Deleted:** Bi

Nikolaos Evangeliou 25/9/2018 12:53
**Deleted:** **A**

Nikolaos Evangeliou 25/9/2018 12:53
**Deleted:** **B**

Nikolaos Evangeliou 25/9/2018 12:53
**Deleted:** **$A_i$**

Nikolaos Evangeliou 25/9/2018 12:54
**Deleted:** **$B_i$**

**Table 3.** Annual prior (ACCMIPv5, EDGAR_HTAPv2.2, MACCity and ECLIPSEv5) and posterior emissions of BC for 2013, 2014 and 2015 (inversion using best representative species and best prior inventory).

| kilotons per year | N. America | N. Europe | N. Siberia | Nenets-Komi | Khanty-Mansiysk |
|---|---|---|---|---|---|
| **2013** | | | | | |
| ACCMIPv5 (prior) | 116 | 241 | 127 | 0.6 | 1.8 |
| EDGAR_HTAPv2.2 (prior) | 117 | 163 | 108 | 0.3 | 0.6 |
| MACCity (prior) | 117 | 244 | 129 | 0.6 | 1.9 |
| ECLIPSEv5 (prior) | 148 | 352 | 187 | 26 | 25 |
| Posterior (ECLIPSEv5) | 149±45 | 152±46 | 230±66 | 17±5 | 32±8 |
| **2014** | | | | | |
| ACCMIPv5 (prior) | 130 | 253 | 178 | 0.5 | 1.9 |
| EDGAR_HTAPv2.2 (prior) | 131 | 175 | 159 | 0.3 | 0.7 |
| MACCity (prior) | 131 | 256 | 179 | 0.5 | 1.8 |
| ECLIPSEv5 (prior) | 162 | 364 | 238 | 25 | 26 |
| Posterior (ECLIPSEv5) | 193±61 | 124±44 | 291±73 | 15±5 | 28±8 |
| **2015** | | | | | |
| ACCMIPv5 (prior) | 149 | 250 | 155 | 0.5 | 1.8 |
| EDGAR_HTAPv2.2 (prior) | 150 | 172 | 136 | 0.3 | 0.6 |
| MACCity (prior) | 150 | 252 | 156 | 0.6 | 1.8 |
| ECLIPSEv5 (prior) | 182 | 381 | 222 | 25 | 25 |
| Posterior (ECLIPSEv5) | 181±55 | 238±66 | 130±52 | 14±5 | 37±8 |
| **3-year average emissions** | **174±58** | **170±59** | **217±69** | **15±5** | **32±8** |

Nikolaos Evangeliou 25/9/2018 12:50
**Formatted:** Font:Not Bold

Nikolaos Evangeliou 25/9/2018 12:50
**Deleted:** Four different optimized emission estimates are given corresponding to use of different prior dataset.

## FIGURES & LEGENDS

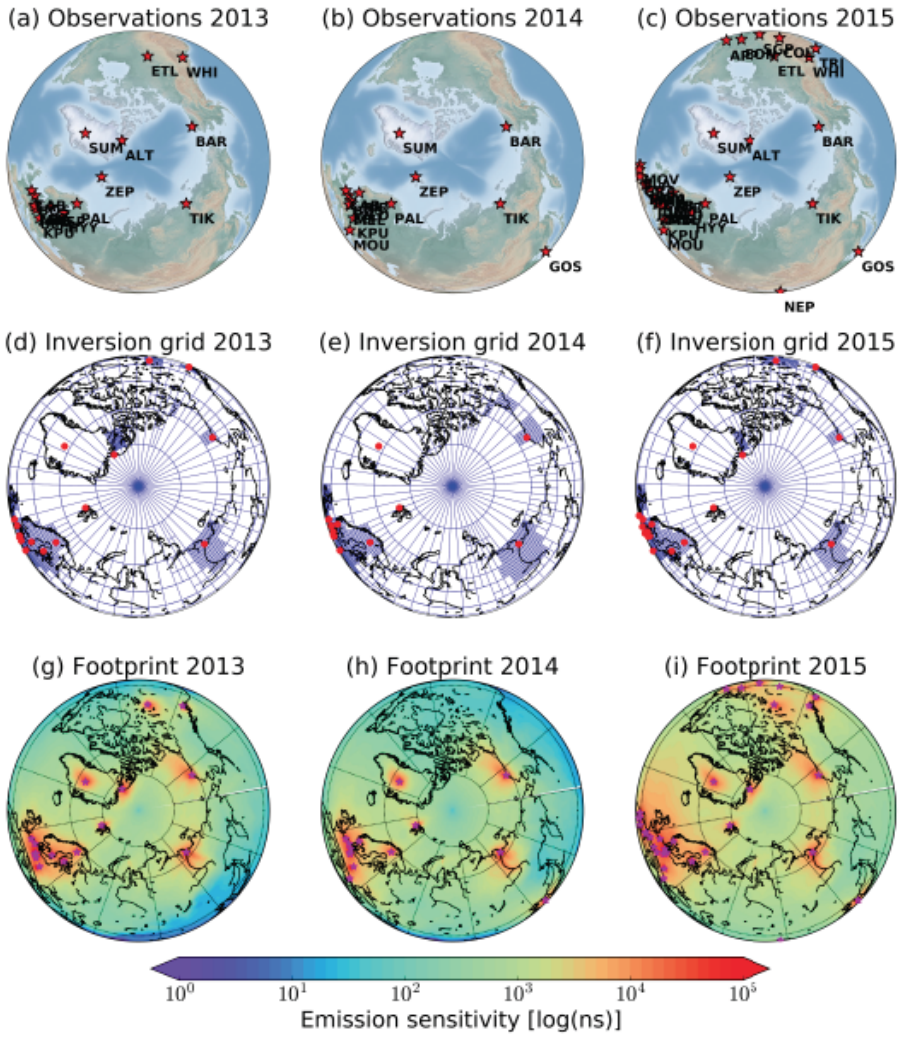


**Figure 1.** Observation network used for the present inversion (a, b and c), and variable-resolution grid used for the inversion (d, e, and f) also showing the location of the observation sites (red stars) for 2013–2015 period. Sensitivity to the surface emissions (i.e., the footprint emission sensitivity or equivalently source-receptor relationship) integrated over all observation sites and all time steps (g, h and i) for the years 2013, 2014 and 2015 (units of log(ns)).

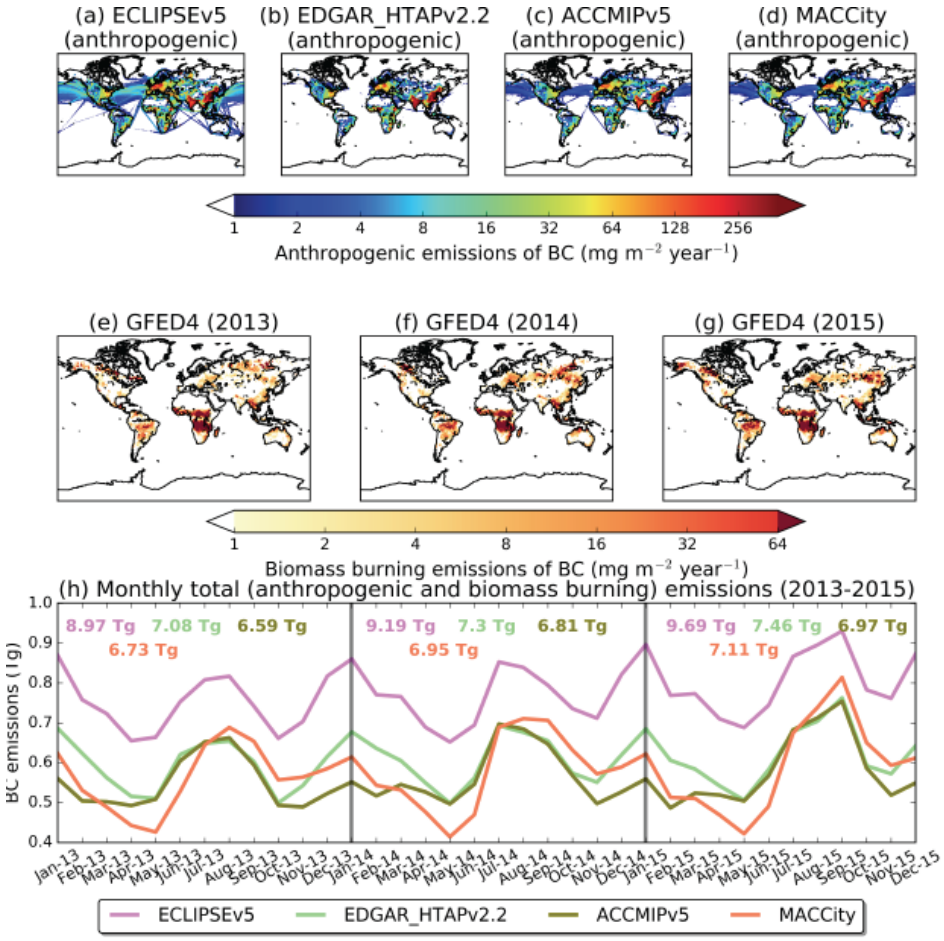


**Figure 2.** (a–d) Anthropogenic emissions of BC in the inversion domain (>50°N) from ECLIPSEv5, EDGAR_HTAPv2.2, ACCMIPv5 and MACCity (anthropogenic emissions are assumed to be constant throughout every year). (e–g) Biomass burning emissions from GFED4 for 2013, 2014 and 2015 (Giglio et al., 2013). (h) Monthly total (anthropogenic and biomass burning) BC emissions north of 50°N from 2013 to 2015 from the four prior inventories used for the inversion. Coloured numbers correspond to total annual BC from each emission inventory.

Nikolaos Evangeliou 25/9/2018 15:24

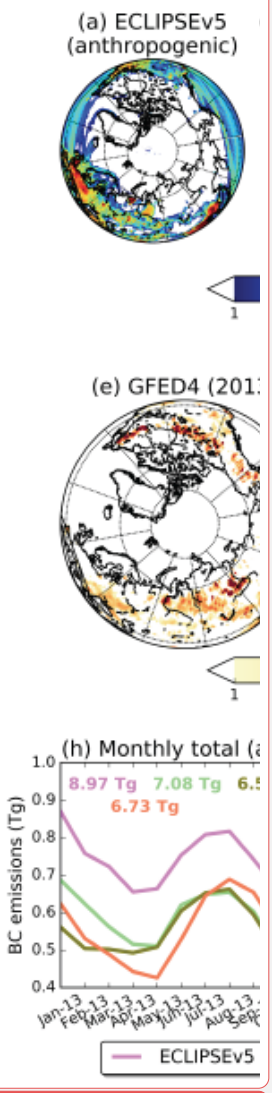


**Deleted:**

Nikolaos Evangeliou 20/9/2018 16:01

**Deleted:** emissions of BC

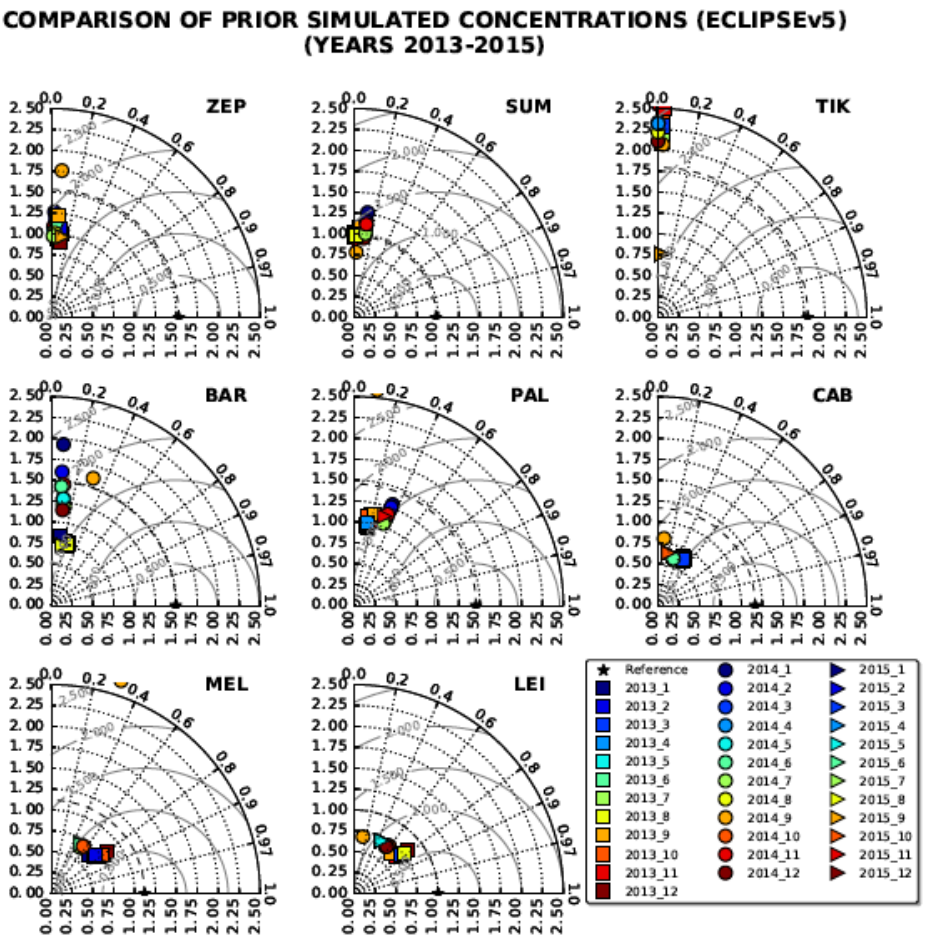


**Figure 3.** Taylor diagrams for the comparison of the prior (ECLIPSEv5) simulated concentrations with observations for all years (2013 – 2015) for 12 BC species with different scavenging coefficients (Table 2). The radius indicates standard deviations normalised against the mean concentration (NSD); the azimuthal angle the Pearson correlation coefficient, while the normalised (against observation) root mean square error (nRMSE) in the simulated concentrations is proportional to the distance from the point on the x-axis identified as "reference" (grey contours).

Nikolaos Evangeliou 27/9/2018 11:26
**Deleted:** Table 2

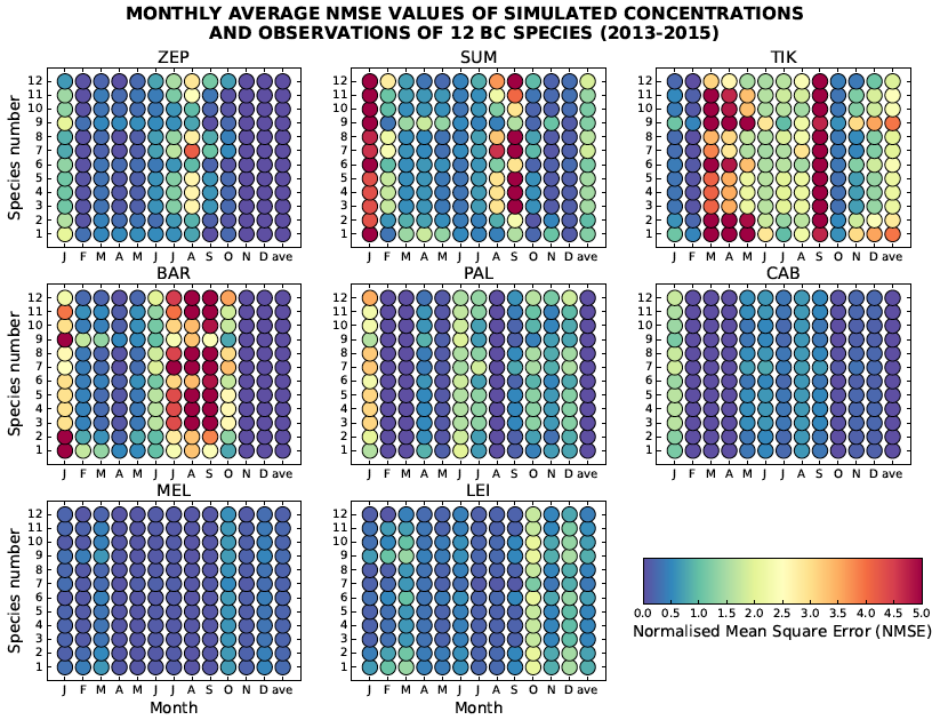


**Figure 4.** Monthly average NMSE values due to use of 12 different BC species defined in Table 2, for the eight stations with complete data in the period 2013–2015. The annual mean is denoted as "ave").

Nikolaos Evangeliou 27/9/2018 11:26
**Deleted:** Table 2

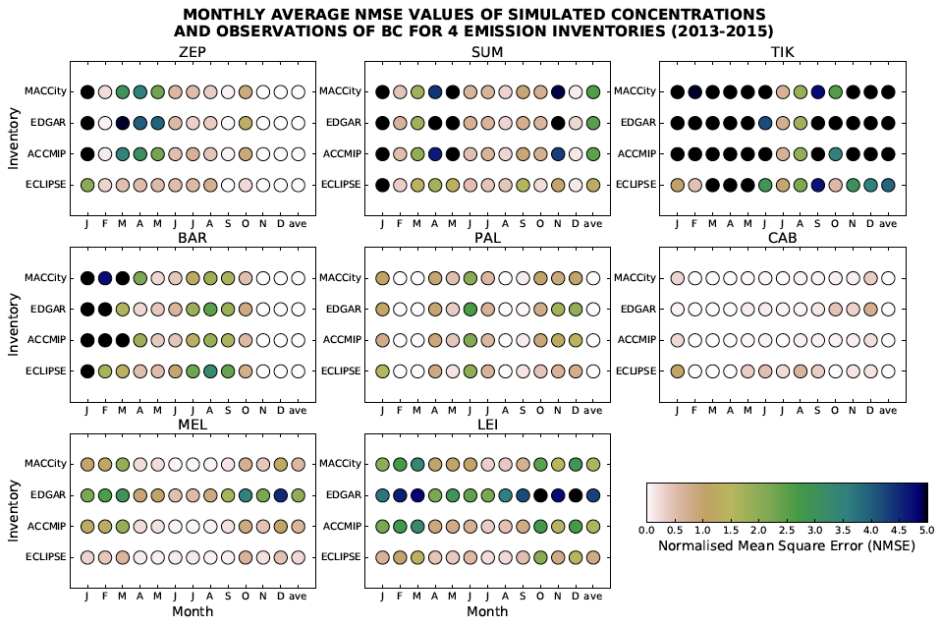


**Figure 5.** Monthly average NMSE values due to use of different emission inventories (ECLIPSEv5, ACCMIPv5, EDGAR_HTAPv2.2, MACCity) for the eight stations with complete data in the period 2013–2015. The annual mean is denoted as "ave").

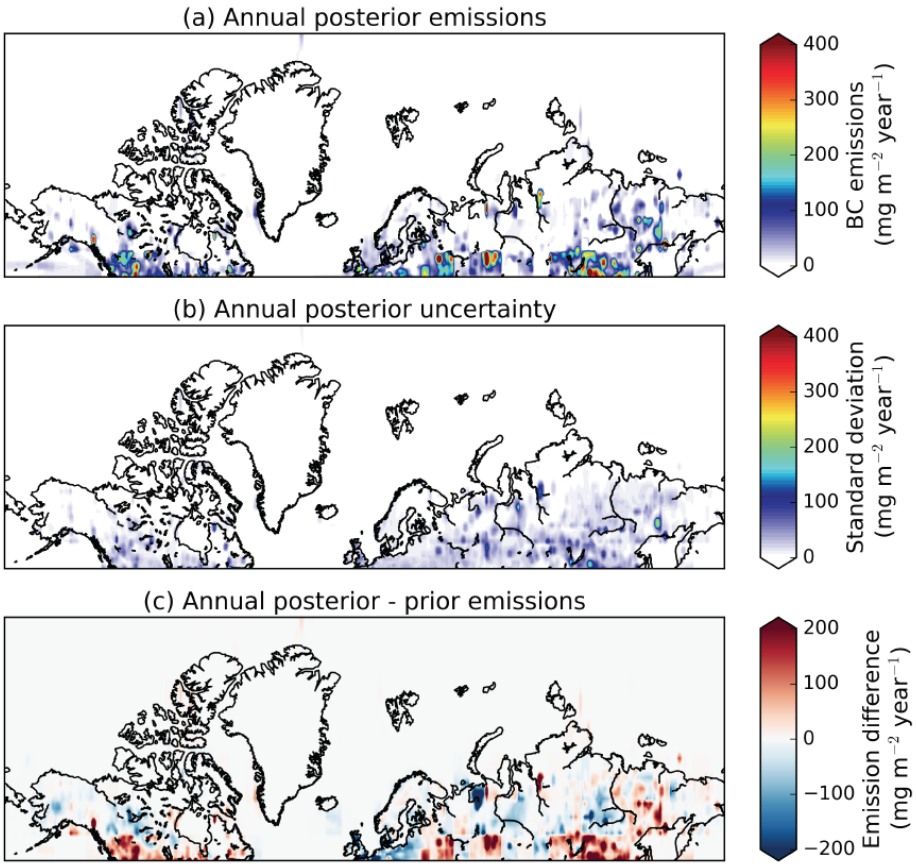


**Figure 6.** (a) Annual posterior emissions of BC in areas >50°N averaged for the period 2013–2015, (b) average posterior uncertainty due to scavenging and use of different prior emissions for the same period. (c) Difference between posterior and prior emissions for 2013–2015.

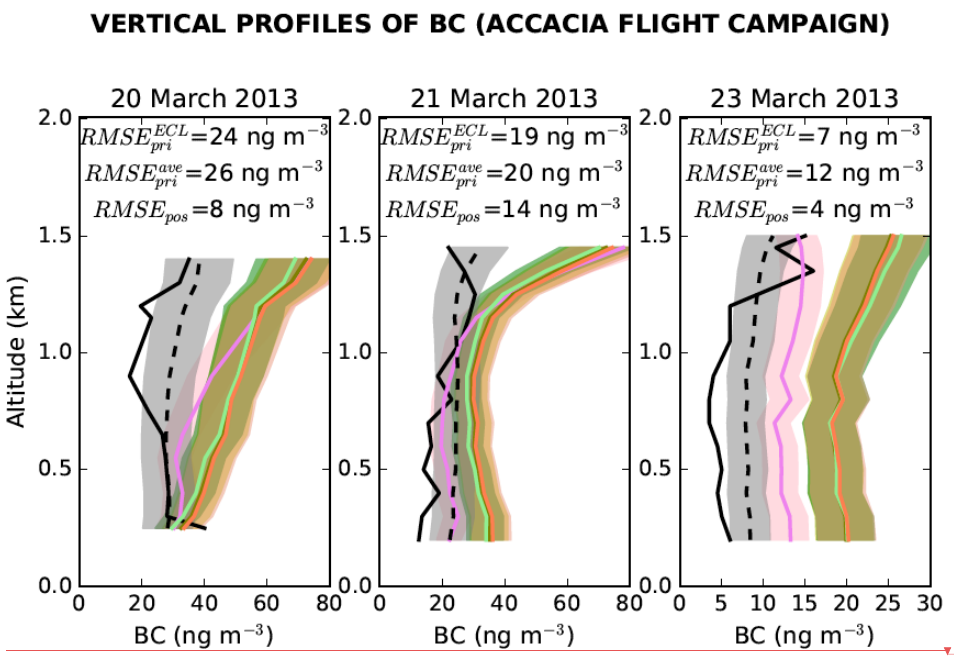


**Figure 7.** Comparison of prior (ECLIPSEv5, ACCMIPv5, EDGAR HTAPv2.2 and MACCity) and posterior simulated concentrations of BC with observations from the ACCACIA flight campaign near Zeppelin station, Ny-Ålesund in 2013 adopted from Sinha et al. (2017). The variability of the prior concentrations (shaded area) was calculated as the standard deviation of BC concentrations from the 12 species with different scavenging coefficients as shown in Table 2. Uncertainties of the posterior concentrations are due to scavenging and use of 4 different a priori datasets (section 3.4). RMSE values are computed for ECLIPSEv5 concentrations, all prior concentrations (average) and posterior simulated BC concentrations.

Nikolaos Evangeliou 25/9/2018 15:23
Deleted:

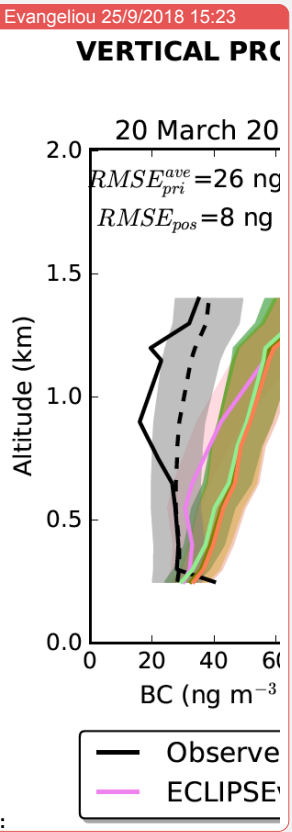


Nikolaos Evangeliou 27/9/2018 11:26
**Deleted:** Table 2

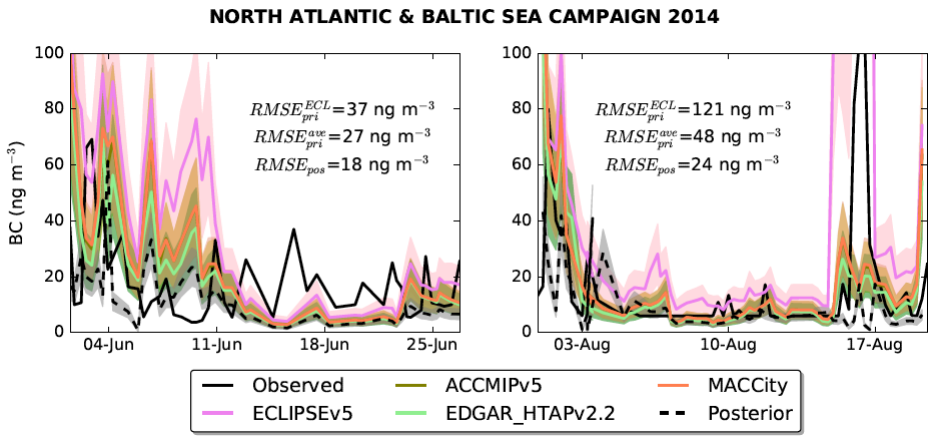


1155

1156 **Figure 8.** Comparison of prior (ECLIPSEv5, ACCMIPv5, EDGAR HTAPv2.2 and
1157 MACCity) and posterior simulated concentrations of BC with observations from a ship
1158 campaign in North Atlantic and Baltic Seas in 2014 adopted from Shevchenko et al. (2016).
1159 The variability of the prior concentrations (shaded area) was calculated as the standard
1160 deviation of BC concentrations from the 12 species with different scavenging coefficients as
1161 shown in Table 2. Uncertainties of the posterior concentrations are due to scavenging and use
1162 of 4 different a priori datasets (section 3.4). RMSE values are computed for ECLIPSEv5
1163 concentrations, all prior concentrations (average) and posterior simulated BC concentrations.

1164

Unknown
**Formatted:** Font:Times New Roman, 12 pt, Not Bold, Font color: Auto

Nikolaos Evangeliou 25/9/2018 15:23
**Deleted:**

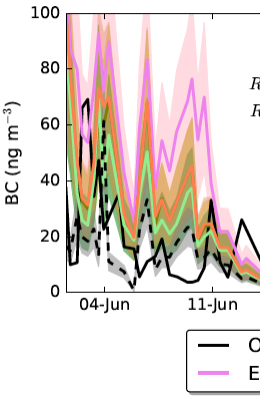


Nikolaos Evangeliou 27/9/2018 11:26
**Deleted:** Table 2

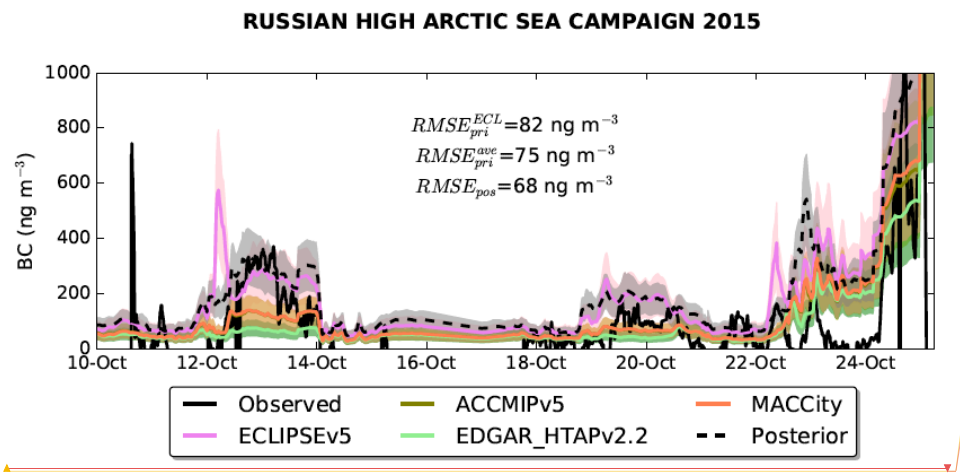


**Figure 9.** Comparison of prior (ECLIPSEv5, ACCMIPv5, EDGAR HTAPv2.2 and MACCity) and posterior simulated concentrations of BC (2015) with observations from a ship campaign in the Russian Arctic in 2015 adopted from Popovicheva et al. (2017). The variability of the prior concentrations (shaded area) was calculated as the standard deviation of BC concentrations from the 12 species with different scavenging coefficients as shown in Table 2. Uncertainties of the posterior concentrations are due to scavenging and use of 4 different a priori datasets (section 3.4). RMSE values are computed for ECLIPSEv5 concentrations, all prior concentrations (average) and posterior simulated BC concentrations.

Unknown
**Formatted:** Font:(Default) Times New Roman

Nikolaos Evangeliou 25/9/2018 15:23
**Deleted:**

Nikolaos Evangeliou 27/9/2018 11:26
**Deleted:** Table 2

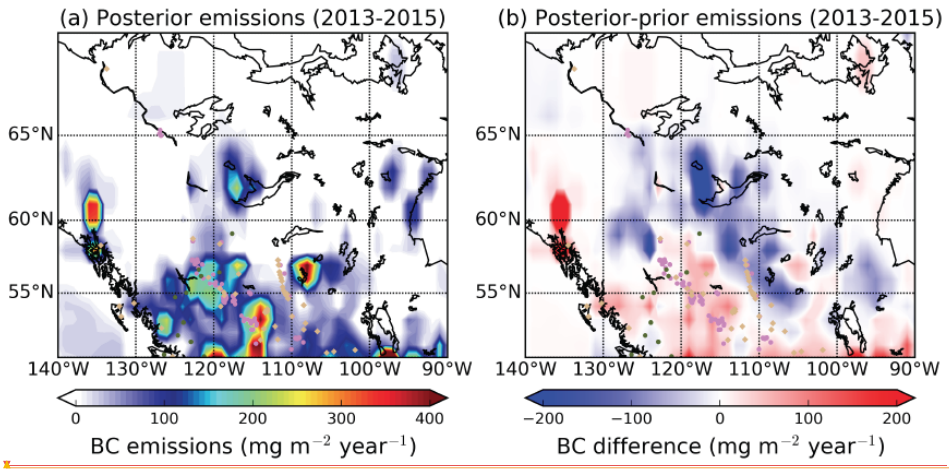


**Figure 10.** (a) Optimised emissions of BC in North America (Western Canada) averaged over the 2013–2015 period. (b) Difference between a posteriori and a priori emissions of BC (ECLIPSEv5 was used as the prior). Magenta points on the map denote the gas flaring industries from the Global Gas Flaring Reduction Partnership (GGFR) (http://www.worldbank.org/en/programs/gasflaringreduction), grey points show the power industries that operate using fossil fuels and oil and gas production and oil refining industries adopted from Industry About (https://www.industryabout.com/canada-industrial-map), while dark green points show active fires from MODIS.

Nikolaos Evangeliou 26/9/2018 12:23
Deleted:
Unknown
**Formatted:** Font:Times New Roman, 12 pt, Not Bold, Font color: Auto

Nikolaos Evangeliou 26/9/2018 12:26
**Deleted:** black

Nikolaos Evangeliou 26/9/2018 12:26
**Deleted:** rectangles

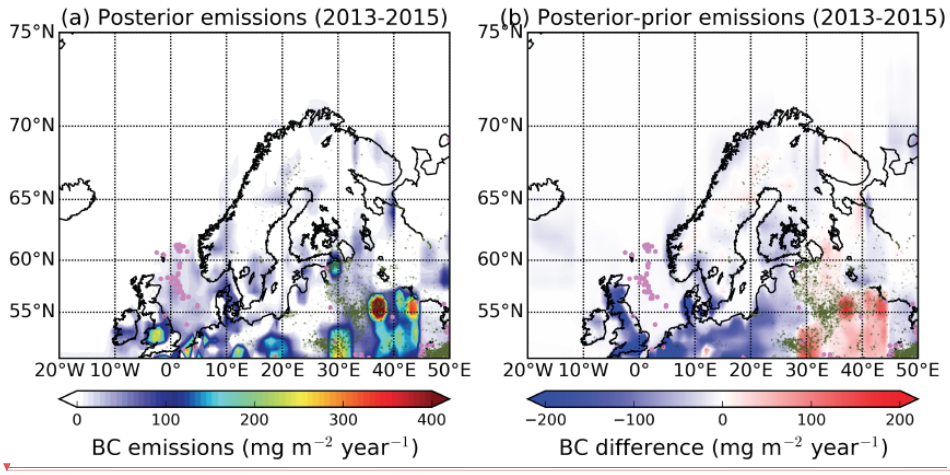


**Figure 11.** (a) Optimised emissions of BC in Northern Europe averaged over the 2013–2015 period. (b) Difference between a posteriori and a priori emissions of BC (ECLIPSEv5 was used as the prior). Magenta points on the map indicate the gas flaring industries from the Global Gas Flaring Reduction Partnership (GGFR) (http://www.worldbank.org/en/programs/gasflaringreduction), while dark green points show the vegetation fires adopted from Hao et al. (2016).

Nikolaos Evangeliou 26/9/2018 12:24

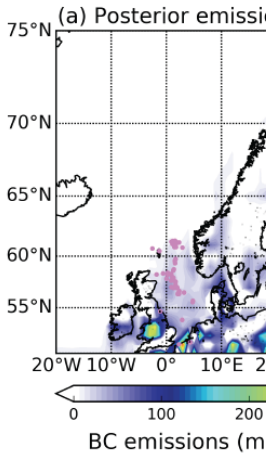


**Deleted:**

Nikolaos Evangeliou 26/9/2018 12:25

**Deleted:** black

Nikolaos Evangeliou 26/9/2018 12:26

**Deleted:** rectangles

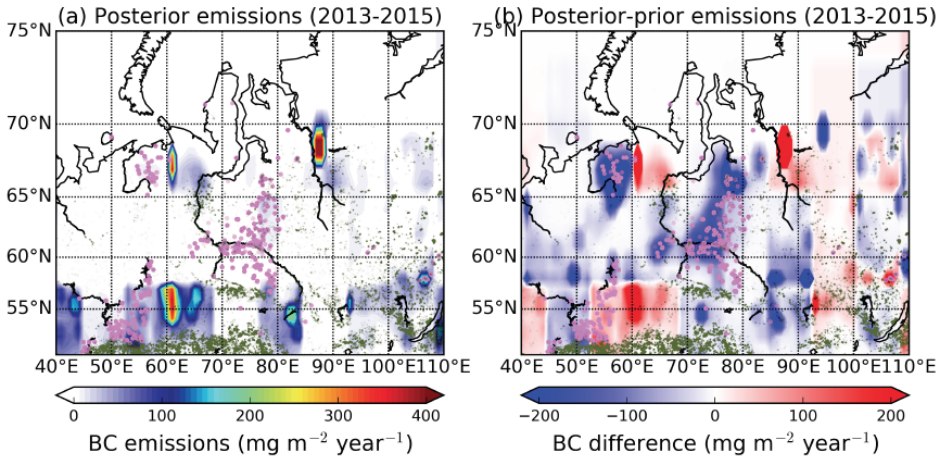


**Figure 12.** (a) Optimised emissions of BC in Western Siberia averaged for the 2013–2015 period. (b) Difference between a posteriori and a priori emissions of BC (ECLIPSEv5 was used as the prior). Magenta points on the map indicate the gas flaring industries from the Global Gas Flaring Reduction Partnership (GGFR) (http://www.worldbank.org/en/programs/gasflaringreduction), while dark green points show the vegetation fires adopted from Hao et al. (2016).

Nikolaos Evangeliou 26/9/2018 12:24

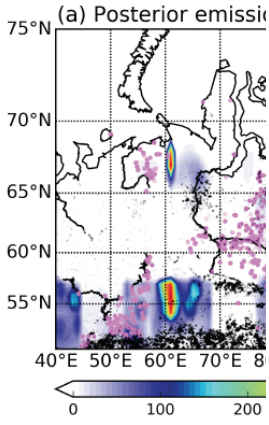


**Deleted:**

Nikolaos Evangeliou 26/9/2018 12:25

**Deleted:** black

Nikolaos Evangeliou 26/9/2018 12:26

**Deleted:** rectangles

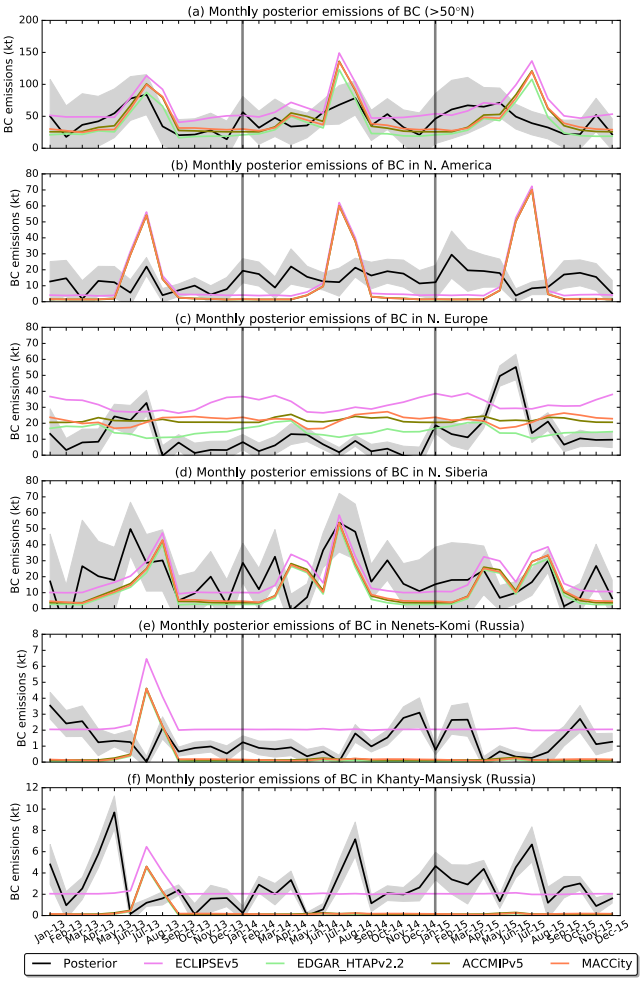


**Figure 13.** Monthly posterior emissions of BC shown for all regions located (a) >50°N, (b) in North America (>50°N), (c) North Europe (>50°N), (d) North Siberia (>50°N), (e) Nenets-Komi oblast (>50°N, Russia) and (f) Khanty-Mansiysk oblast (>50°N, Russia) for the 2013–2015 period. Monthly prior emissions of BC from ECLIPSEv5, EDGAR_HTAPv2.2, ACCMIPv5 and MACCity emissions inventories are also shown for the same regions and time period. The uncertainty of the posterior emissions of BC stems from the use of different scavenging coefficients and different prior emission datasets (see section 3.3).

Nikolaos Evangeliou 26/9/2018 13:50

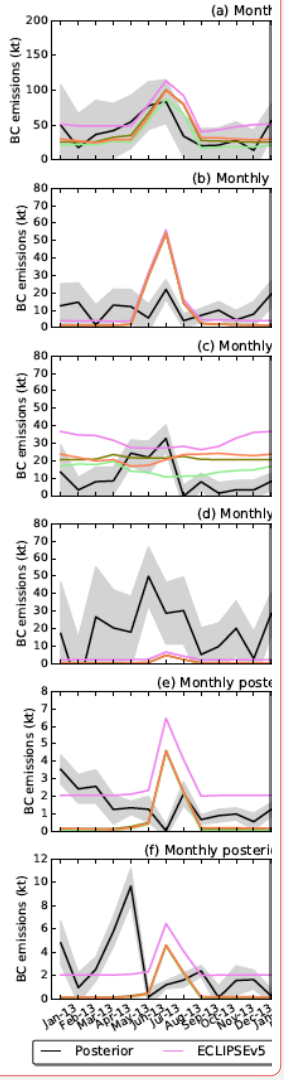

**Deleted:**

## SUPPLEMENTARY FIGURES & LEGENDS

**Figure S 1.** Taylor diagrams for the comparison of the prior simulated concentrations with observations for all years (2013 – 2015) for 12 BC species with different scavenging coefficients (Table 2). The radius indicates standard deviations normalised against the mean concentration (NSD); the azimuthal angle the Pearson correlation coefficient, while the normalised (against observation) root mean square error (nRMSE) in the simulated concentrations is proportional to the distance from the point on the x-axis identified as "reference" (grey contours). The results refer to the use of ACCMIPv5, EDGAR_HTAPv2.2 and MACCity as the prior emissions.

Nikolaos Evangeliou 27/9/2018 11:26
**Deleted:** Table 2

**Figure S 2.** Monthly average relative model-observation mismatches ($[\boldsymbol{model - observations}]/\boldsymbol{observations}$) for prior simulated (average values from all four inventories used) concentrations of BC due to the perturbation of scavenging parameters according to Table 2 for the inversions of 2013, 2014 and 2015.

Nikolaos Evangeliou 27/9/2018 11:26
**Deleted:** Table 2

**Figure S 3.** Monthly average model-observation mismatches ($[\boldsymbol{model - observations}]/\boldsymbol{observations}$) for prior simulated concentrations of BC (best species) due to use for four different emission inventories (ECLIPSEv5, ACCMIPv5, EDGAR_HTAPv2.2 and MACCity) for the inversions of 2013, 2014 and 2015.

**Figure S 4.** Taylor diagrams for the comparison of the posterior simulated concentrations with observations for all years (2013 – 2015). The radius indicates standard deviations normalised against the mean concentration (NSD); the azimuthal angle the Pearson correlation coefficient, while the normalised (against observation) root mean square error (nRMSE) in the simulated concentrations is proportional to the distance from the point on the x-axis identified as "observed" (grey contours).

**Figure S 5.** (a, c, e) Optimised emissions of BC in North America (Western Canada) for 2013, 2014 and 2015. (b, d, f) Difference between a posteriori and a priori emissions of BC (ECLIPSEv5 was used as the prior). Magenta points on the map denote the gas flaring industries from the Global Gas Flaring Reduction Partnership (GGFR)

(http://www.worldbank.org/en/programs/gasflaringreduction), grey points show the power industries that operate using fossil fuels and oil and gas production and oil refining industries adopted from Industry About (https://www.industryabout.com/canada-industrial-map), while dark green points show active fires from MODIS.

Nikolaos Evangeliou 26/9/2018 12:55
**Deleted:** black rectangles

**Figure S 6.** (a, c, e) Optimised emissions of BC in Northern Europe for 2013, 2014 and 2015. (b, d, f) Difference between a posteriori and a priori emissions of BC (ECLIPSEv5 was used as the prior). Magenta points on the map indicate the gas flaring industries from the Global Gas Flaring Reduction Partnership (GGFR) (http://www.worldbank.org/en/programs/gasflaringreduction), while dark green points show vegetation fires adopted from Hao et al. (2016).

Nikolaos Evangeliou 26/9/2018 12:55
**Deleted:** black rectangles

**Figure S 7.** (a, c, e) Optimised emissions of BC in Western Siberia for 2013, 2014 and 2015. (b, d, f) Difference between a posteriori and a priori emissions of BC (ECLIPSEv5 was used as the prior). Magenta points on the map indicate the gas flaring industries from the Global Gas Flaring Reduction Partnership (GGFR) (http://www.worldbank.org/en/programs/gasflaringreduction), while dark green points show forest fires adopted from Hao et al. (2016).

Nikolaos Evangeliou 26/9/2018 12:55
**Deleted:** black rectangles